

# BARC

## NEWSLETTER

### IN THIS ISSUE

- Drop-Interface Coalescence in liquid-liquid Systems: Effect of Surface Active Agents
- Proton Beam Set-up for Radiobiological Studies
- High Temperature Deformation Behavior of Nb-1Zr and Nb-1Zr-0.1C
- Development of Quick Scan Whole Body Monitor for *in-vivo* Monitoring of Radiation Workers and General Public
- Development of Ce doped  $\text{Li}_6\text{Y}(\text{BO}_3)_3$  Crystal Based Portable Solid State Detectors for Thermal Neutrons



*Celebrating the spirit of Diamond Jubilee Year*  
Department of Atomic Energy Tableau in the 66<sup>th</sup> Republic Day Parade 2015 at Rajpath, New Delhi



### **Atoms in the Service of the Nation**

*Celebrating its diamond jubilee year, the Department of Atomic Energy portrays in its tableau, its expertise in harnessing the tremendous potential of the atom for societal benefits in the service of the nation. The tableau is led by a white dove atop an atomic orbital symbolising the conviction of the nation to spread the message - 'Atoms for Peace'. It also pays a somber homage to the visionary Dr. Homi Jehangir Bhabha, founding father of the Indian Nuclear Programme. The trailer portion is conceptually divided into three parts depicting peace, progress and prosperity, vis-a-vis the service deliverables of the Department. The first part symbolises progress in the field of medical technology depicting the indigenously developed 'Bhabhatron' machine, used in radio-therapy and delivering affordable healthcare. The colourful flora, following it, posturizes prosperity in food and agriculture through mutation breeding technology to provide disease resistant and high yielding seeds; food irradiation techniques that increase the shelf life of the produce. Lastly, standing tall, the indigenous Nuclear Reactor showcases the advantage of nuclear energy to provide an unlimited supply of clean and green energy for the sustained progress of the nation.*

**-DEPARTMENT OF ATOMIC ENERGY**

## CONTENTS

### Brief Communications

- Apprehensions about Inhalation Exposures due to Radon ( $^{222}\text{Rn}$ ) and Thoron ( $^{222}\text{Rn}$ ) in High Background Radiation Areas of India iii
- Facility for Time Resolved Raman Spectroscopy of Materials Under Shocks v

### Research Articles

- Drop-Interface Coalescence in liquid-liquid Systems: Effect of Surface Active Agents 1  
S. Dixit, S. Mukhopadhyay and K.T. Shenoy  
Chemical Engineering Division  
and  
V.A. Juvekar  
Indian Institute of Technology Bombay, Mumbai
- Proton Beam Set-up for Radiobiological Studies 5  
N.N. Bhat and B.K. Sapra  
Radiological Physics and Advisory Division  
and  
S.K. Gupta  
Ion Accelerator Development Division
- High Temperature Deformation Behavior of Nb-1Zr and Nb-1Zr-0.1C 8  
R. Kapoor, A.N. Behera, A. Sarkar and J.K. Chakravartty  
Materials Group

### Technology Development Articles

- Development of Quick Scan Whole Body Monitor for in-vivo Monitoring of Radiation Workers and General Public 13  
Rajesh Sankhla, I.S. Singh, D.D. Rao and K.S. Pradeepkumar  
Radiation Safety Systems Division
- Development of Ce doped  $\text{Li}_6\text{Y}(\text{BO}_3)_3$  Crystal Based Portable Solid State Detectors for Thermal Neutrons 20  
A.K. Singh, M. Tyagi, S.G. Singh, D.G. Desai, B. Tiwari,  
S. Sen, S.C. Gadkari and S.K. Gupta  
Technical Physics Division

### News & Events

- Special Session on the Eve of 100<sup>th</sup> Meeting of Conventional & Fire Safety Review Committee (CFSRC) of BARC Safety Council (BSC) 25
- Technology Transfer to Industries 27

### BARC Scientists Honoured

## Editorial Committee

### Chairman

Dr. S.M. Sharma  
Director, Physics Group

### Co-Chairman

Dr. G.K. Dey  
Associate Director, Materials Group

### Editor

Dr. G. Ravi Kumar  
Head, SIRD

### Associate Editors for this issue

Dr. S.M. Yusuf, SSPD  
Dr. B.K. Sapra, RP&AD

### Members

Dr. G. Rami Reddy, RSD  
Dr. A.K. Tyagi, ChD  
Dr. S.M. Yusuf, SSPD  
Dr. S. Kannan, FCD  
Dr. C.P. Kaushik, WMD  
Dr. S. Mukhopadhyay, SD  
Dr. A.K. Bhattacharjee, RCnD  
Dr. B.K. Sapra, RP&AD  
Dr. J.B. Singh, MMD  
Dr. K.G. Bhushan, TPD  
Dr. S. Mukhopadhyay, ChED  
Dr. S.K. Sandur, RB&HSD  
Dr. (Smt.) S.C. Deokattey, SIRD

## From the Editor's Desk

The fourth issue of the BARC Newsletter for the year 2015 is in front of you. This time we publish five articles and two Brief Communications, each highlighting various areas of R&D in BARC.

A facility has been set up recently for proton beam therapy applications and biomarker studies. This will provide an opportunity to explore the effects of proton beam on model cellular systems. A brief report of this facility has been featured in this issue. On similar lines, another research article details the development of a system for monitoring of personnel who are exposed to radiation. The Quick Scan Whole Body Monitor (QS-WBM) has been designed, fabricated and commissioned at BARC to quickly and efficiently monitor internal contamination of radiation personnel.

The Founder's Day Special Issue of the BARC Newsletter was released by Director, BARC on 29<sup>th</sup> October, 2015. We would like to thank all our contributors for sending their award winning papers for the issue which carried 47 papers.

We invite both brief reports as well as full-fledged articles of recent research and new developments from all Divisions of BARC.



Dr. G. Ravi Kumar  
On behalf of the Editorial Committee

# Apprehensions about Inhalation Exposures due to Radon ( $^{222}\text{Rn}$ ) and Thoron ( $^{220}\text{Rn}$ ) in High Background Radiation Areas of India

Health, Safety and Environment Group

The population groups exposed to significantly higher levels of natural background radiation than the average worldwide, have been surveyed extensively the world over, to assess the radiation-induced health effects, if any, of low dose rate radiation exposures. The designated HBRAs in India are the monazite sand bearing regions along the long coastline spanning over Ullal in Karnataka, coastal parts of Tamilnadu and Kerala and southern coast of Odisha. The HBRAs of Kerala experience terrestrial gamma radiation of upto 70 mSv a year, which is significantly higher than in Normal Background Radiations Areas (NBRAs). However, epidemiological and cytogenic studies carried out on these populations have not shown any detrimental health effects attributable to radiation (Nair et al., 2009, Koya et al, 2012).

The total radiation dose received by the populations is a sum of the external and the internal (ingestion + inhalation) dose. Several dosimetric surveys in the HBRAs of Kerala have been carried out to estimate the external dose due to gamma rays. Inhalation dose, which is a significant component (~55%) of the total radiation dose received by the populations, arises due to radon ( $^{222}\text{Rn}$ ), thoron ( $^{220}\text{Rn}$ ), and their progenies which are members of the  $^{238}\text{U}$  and  $^{232}\text{Th}$  radioactive decay series. An attempt to estimate the indoor inhalation dose by

measuring the radon and thoron gas concentration in some villages of Kerala was made by Chougaonkar et al., 2004 and Pereira et al., 2012 using the twin cup dosimeters. The inhalation doses were based on derived estimates of the progeny concentrations inferred from the measured gas concentrations, for want of a technique to directly determine

the long-term progeny concentrations. This methodology is error-prone because it requires the use of equilibrium factor (EF), for which the default value (~0.4 for  $^{222}\text{Rn}$ ) is used. However, EF is very sensitive to air exchange rates, and prevalent aerosol concentrations. Moreover, the concept of EF is invalid for  $^{220}\text{Rn}$  as it has a very short half-life of 55 s. Any slight changes in the ventilation patterns can change the EF for  $^{220}\text{Rn}$  from 0.0001 to 0.1. This necessitates the simultaneous measurements of the gases and their progenies contributing to the inhalation dose.

This long-standing need of simultaneous measurements of  $^{222}\text{Rn}$  and  $^{220}\text{Rn}$  gas along with their respective progeny was made possible with the in-house development of deposition based Direct Radon/Thoron Progeny Sensors (Mishra et al., 2008, 2009). These are energy degrader mounted SSNTDs (LR-115), that selectively register the alpha particles emitted from the deposited progeny atoms on the surface of the detectors. Moreover, the errors in the measurement of the gas concentrations were considerably reduced by the development of the improved pin-hole twin cup dosimeter (Sahoo et al., 2013). These two passive detectors (Fig. 1) were deployed biannually in around 800 houses of HBRAs of Odisha and Kerala during 2010 to 2012 to assess



Fig.1: Detectors used for measurement of  $^{220}\text{Rn}$  and  $^{222}\text{Rn}$  gas and progeny concentrations

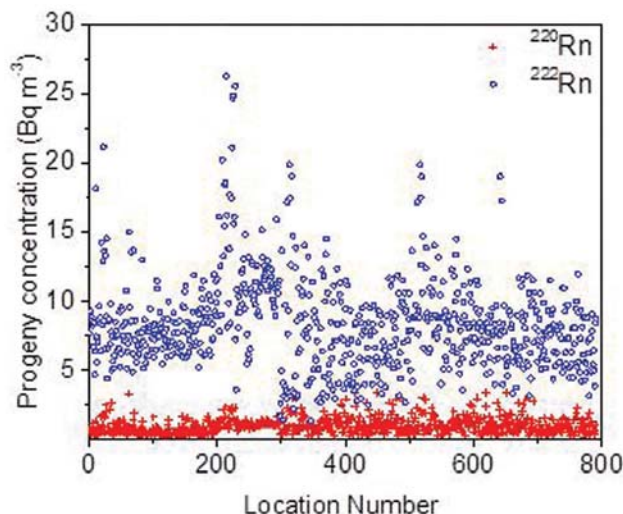


Fig. 2: Scatter graph showing  $^{220}\text{Rn}$  and  $^{222}\text{Rn}$  progeny concentrations in HBRAs of Kerala and Odisha

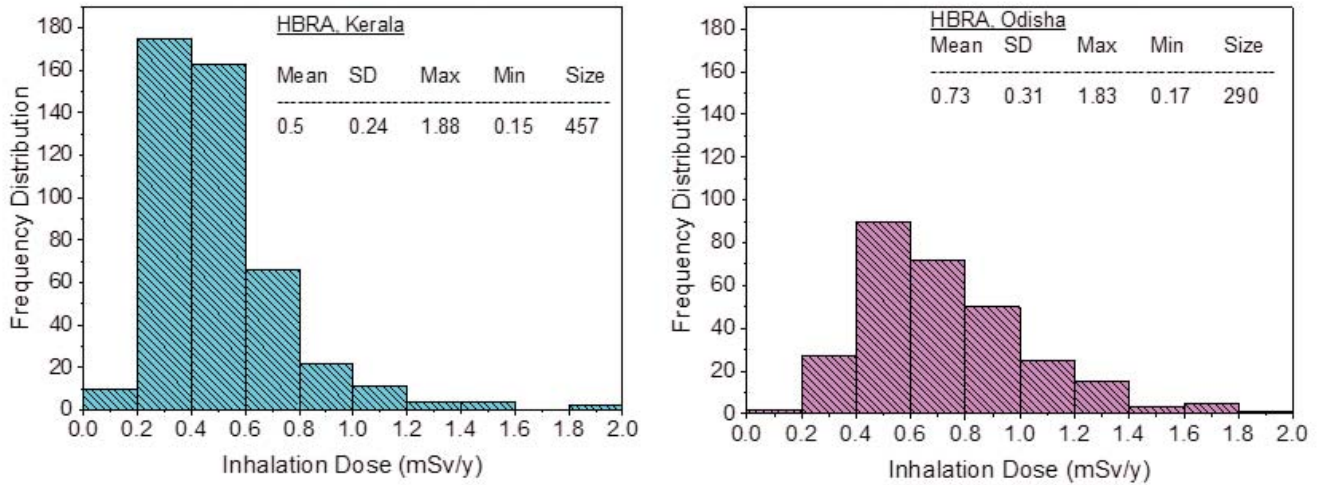


Fig.3: Inhalation Dose profiles of HBRA of Kerala and Odisha

the inhalation doses. The study region covered five villages of Karunagapally Taluk of Kollam district in Kerala and 10 villages of Ganjam district in Odisha. Since the gamma dose rates in these areas are appreciably higher than in NBRAs, it was of interest to examine whether the levels of inhalation doses received indoors are also similarly higher. The study showed that gamma dose rate levels lie in the range of 0.1 - 2  $\mu\text{Sv h}^{-1}$  with a mean of about 0.5  $\mu\text{Sv h}^{-1}$  (as a comparison the value for Mumbai is  $\sim 0.06\text{-}0.1 \mu\text{Sv h}^{-1}$ ). Based on the measurements of  $^{222}\text{Rn}$  and  $^{220}\text{Rn}$  progeny concentrations (Fig. 2), the average inhalation dose was estimated as 0.5 mSv/y and 0.7 mSv/y respectively in HBRA of Kerala and Odisha (Fig. 3) which is very similar to that observed in NBRAs (Mayya et al., 2012, Avinash et al., 2014).

The study brings out the fact that even though the HBRA in India have external gamma effective doses which are about 10 times higher than the NBRAS, yet the inhalation doses due to radon, thoron and their progeny are similar to that observed in normal background regions. The reason for this finding is that the gamma radiations, emitted from thorium bearing subjacent earth, being highly penetrating, reach the indoor environment imparting an external dose to the residents. But, radon and thoron which are gaseous in nature, can enter the indoor environment only via cracks on the floor of the houses. So, in a way, the indoor flooring provides a shield against the entry of radon and thoron, in the same way as in indoors of NBRAS. In addition, as the year round temperature in these areas is 30-35°C, these houses are generally well ventilated, which does not permit buildup of these radioactive gases and their decay product in indoor environments. It was also observed that the local sands

were not used as building materials, and floorings were concrete, leading to negligible contribution from the building materials. This important finding has far reaching implications, especially for epidemiological studies.

- Rosaline Mishra and B.K. Sapra

**References**

1. Avinash P. R., Rajesh S., Kerur B. R., Mishra Rosaline. India, *J Radioanal Nucl Chem* (2014) 302:1321–1326.
2. Chougankar M.P., K.P. Eappen, T.V. Ramachandran, P.G. Shetty, Y.S. Mayya, S. Sadasivan, S. Venkat, V. Raj., India. *J Environ Radioact*, 71 (2004), pp. 275–297.
3. Koya P. K. M., Chougankar M. P., Predeep P., Jojo P. J., Cheriyan V. D., Mayya Y. S., Seshadri M. *Radiation Research* (2012), 177(1),109-16
4. Mayya Y.S., Mishra, R., Prajith, R., Gole, A. C., Sapra, B. K., Chougankar, M. P., Nair, R. R. K., Ramola, R. C., Karunakara, N. and Koya, P. K. M.. *Radiation Protection Dosimetry* (2012), 152(1–3), 18 –24.
5. Mishra Rosaline and Mayya Y. S., *Radiation Measurements* (2008), 43, 1408-1416.
6. Mishra Rosaline, Mayya Y. S., Kushwaha H. S., *Journal of Aerosol Science* (2009), 40, 1-15.
7. Nair Raghu Ram K., Rajan Balakrishnan, Akiba Suminori, Jayalekshmi P., Nair M Krishnan, Gangadharan P., Koga Taeko, Morishima Hiroshige, Nakamura Seiichi, Sugahara Tsutomu, *Health Physics* (2009) 96(1), 55-66.
8. Pereira, C.E., Vaidyan, V.K., Chougankar, M.P., Mayya, Y.S., Sahoo, B.K., Jojo, P.J. *Radiat Prot Dosimetry* (2012), 150(3), 385-90.
9. Sahoo, B. K. et al. *Radiation Measurements* (2013) 58, 52-60.

## Facility for Time Resolved Raman Spectroscopy of Materials Under Shocks

Physics Group

High pressure and synchrotron radiation physics division is engaged in studies of materials behaviour under extreme conditions by using lasers for shock (dynamic) compression and diamond anvil cell (DAC) for static compression. In case of dynamic compression, we have achieved Equation-of-State (EOS) of materials (PVA, Al, Titanium, Cu, Au etc.) upto 30 Mbar using optical streak camera and interferometry/ shadowgraphy setup. This technique provides end state information only in terms of shock velocity and particle velocity. It cannot provide information at molecular level. Such an information is obtainable in static pressure conditions through spectroscopic measurements but, so far, was not possible under shock conditions. We have now developed a new facility (Time resolved Raman spectroscopy setup) which enables us to study the materials behaviour at molecular level under dynamic pressure conditions. This facility has been successfully commissioned and optimized for various solid (PTFE, PMMA, Polystyrene etc.) and liquid samples ( $\text{CCl}_4$ , benzene,  $\text{CS}_2$  etc.).

This technique is based on pump probe experiment. Schematic layout and photograph of facility are shown

in figure 1. We have used 2J/8ns Nd:YAG laser system which is designed to deliver two laser pulses simultaneously one each for pump (Shock generation @ 1064 nm) and probe (Raman excitation @ 532 nm) respectively. The Raman scattered signal was measured by a half meter Raman spectrometer with gateable ICCD camera. The resolution of the spectrometer is  $2 \text{ cm}^{-1}$  and ICCD camera gate pulse can go down to 1.2 ns.

The target was mounted in confinement geometry which consists of a cover glass ( $100 \times 100 \times 5 \text{ mm}^3$ ), an Aluminium foil of thickness 25-50  $\mu\text{m}$  for shock build-up, followed by the target to be studied (PTFE in this case) and a backup glass ( $100 \times 100 \times 5 \text{ mm}^3$ ). The whole assembly was mounted on a motorized X-Y-Z stage which was synchronized with the laser pulse to achieve every shot on fresh target.

A detailed Raman study of Polytetrafluoroethylene (PTFE) at various shock pressures and time delays has been done. Figure 2a shows the symmetric stretching mode of  $\text{CF}_2$  ( $729 \text{ cm}^{-1}$ ) at a delay of 38 ns between pump and probe beam. A blue shift of  $12 \text{ cm}^{-1}$  @  $729 \text{ cm}^{-1}$  was observed at a pressure of 2.4 GPa which

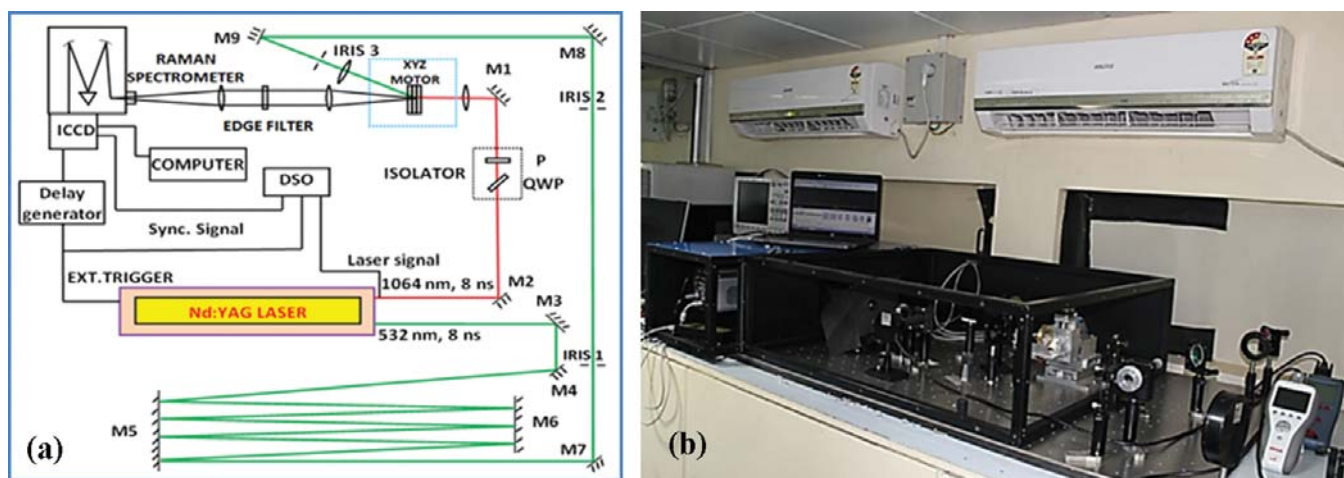


Fig.1: (a). Schematic and (b). Photograph of experimental setup of Time Resolved Raman Spectroscopy

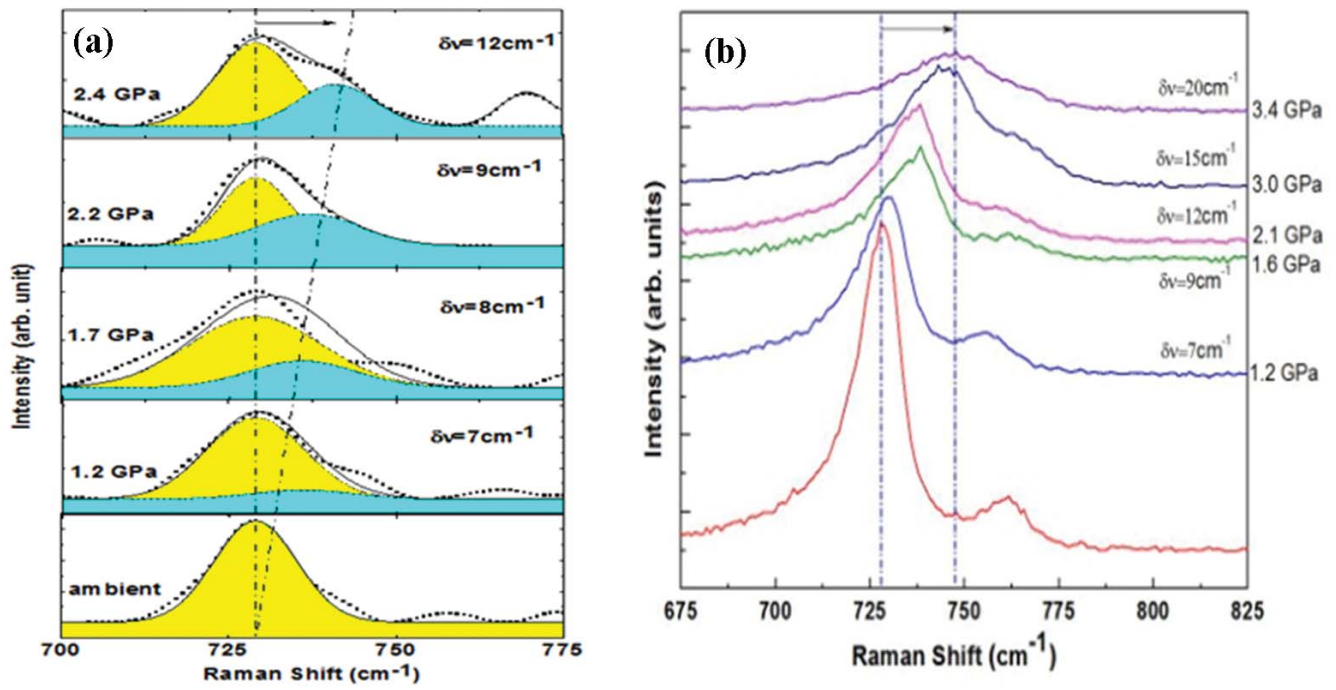


Fig. 2: Raman spectra of PTFE at various pressure in (a) Dynamic compression

is slightly lower than the data measured under static pressures as shown in figure 2b. This difference may

be due lesser laser absorption in targets and also temperature effect cannot be ruled out.

# Drop-Interface Coalescence in liquid-liquid Systems: Effect of Surface Active Agents

S. Dixit, S. Mukhopadhyay and K.T. Shenoy  
Chemical Engineering Division

and

V.A. Juvekar  
Indian Institute of Technology Bombay, Mumbai

## Abstract

*Coalescence will usually occur, when a drop approaches a two phase interface, where an interfacial film forms, drains to a certain thickness and then ruptures. Film rupture is very rapid, and so most of the time taken for the coalescence of a drop to occur is the coalescence time. In the present work, time of fall of drop of aqueous phase through an organic pool and its coalescence with its bulk phase has been studied with a typical liquid-liquid extraction system. Effect of surface active agents/ emulsifiers on coalescence has been studied.*

## Introduction

Coalescence of drops, suspended in a liquid, plays a crucial role in mass transfer contactors. In a mass transfer contactor, efficient dispersification is required to enhance the transport efficiency. On the other side, adequate coalescence of drops is required to reduce emulsification and entrainment losses during phase separation. Emulsification results in poor disengagement of the two phases leading to an inefficient extraction, loss of control on phase ratio and significant entrainment losses. In the most conventional extraction systems, the interface contains interfacially active contaminants. These contaminants modify the interfacial properties, which resist the film drainage and hence retard coalescence. Effects of interfacial properties on coalescence have not been systematically studied for the solvent extraction systems relevant to the department. In liquid membrane based mass transfer contactors, like hollow fiber modules, emulsifiers are often added to stabilize the dispersion during transport. Type and concentration of emulsifier play a crucial role in coalescence of the drops during phase separation in such systems.

A simple technique for studying the rate of coalescence is to measure the "coalescence time". When a drop of liquid 1 approaches through an immiscible liquid 2 to the interface of phases 1 and 2, it takes rest at the interface before merging with its bulk phase. The time interval, during which the drop rests at the interface, is known as the coalescence time. In the present work, time of approach of a drop of an aqueous phase through an organic phase and its coalescence time with its bulk phase have been studied using high speed

camera and illumination system. Emulsifiers play an important role in modulating the coalescence time. Role of emulsifier coupled with the extractant having surface activity has also been seen.

## Methodology

The experimental set-up for the present study on drop-drop coalescence under gravitational field consists of a cuvette fixture, in which organic and aqueous phases have been poured to form a liquid-liquid interface. The set-up consists of an auto syringe to release the drop of aqueous phase in organic continuum, illumination system and a high speed camera. Images are taken for drop travelling through the organic pool, sitting on organic-aqueous interface and then merging with its bulk phase. The time of approach of drop of aqueous phase through organic phase as well as the coalescence time of drop with its bulk phase have been observed for different compositions. The organic phase is taken as TBP (0%, 5%, 10%, 20% and 30% v/v) dissolved in dodecane with and without emulsifier SPAN 80 (3 % v/v), while the aqueous phase was distilled water.

## Theoretical

**A) Deformation of a drop:** The deformation of a drop under a compressive force is estimated by considering it to be contained in a fluid between two parallel planes, which are pushed together with a force according to Charles and Mason. For deformation, weight of the drop overcomes the interfacial tension force of the drop, as interfacial forces holding the drop together. At equilibrium, resultant of gravitational and buoyant force should be equal to interfacial tension force for a given distortion,

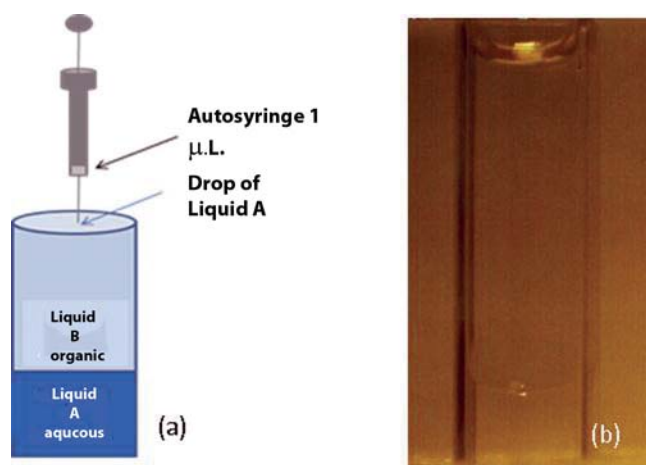


Fig. 1: a) Schematic of the experimental facility, b) video image of the drop resting at the interface

$$\frac{4}{3}\pi b^3 g \Delta\rho = \sigma \pi c^2 \frac{2}{b} \tag{1}$$

$$c = b^2 \left[ \frac{2\Delta\rho g}{3\sigma} \right]^{1/2} \tag{2}$$

Where,  $b$  is the radius of undistorted spherical drop and  $c$  is the radius of flat disc formed on the top and bottom, after the drop is deformed.  $\Delta\rho$  is the difference in the density of the drop and the surrounding medium. From above equations, force required to produce a given distortion increases with interfacial tension  $\sigma$  and drop curvature  $1/b$ . Liquid film trapped between the interface is plano-convex in shape and is thinnest along the circumference of a circle of radius  $c$  according to Gillespie and Rideal.

**B) Thinning of the film:** Following Assumptions are involved for the thinning of the film of continuous phase according to Reynolds; a) Space between the drop and the two phase interface is so small that the motion of fluid is assumed to be free from eddies i.e. laminar flow. b) Forces arising from weight and inertia are altogether small compared with the stresses arising from viscosity. c) Flow is radial i.e.  $z$ -component of fluid velocity is zero.

The close approach of surfaces immersed in a viscous fluid in response to a constant force  $F$  has been considered. Separation at any time  $t$  is given by  $z = h$  at  $r = 0$ . At a distance  $r$  from the origin, separation is  $\xi$ , which is function of  $r$ . Velocity of approaching surface at time  $t$  is  $V = -dh/dt$ . During approach, incompressible fluid of viscosity  $\eta$  is expelled radially from between the two surfaces at a velocity  $u(z,r)$ . Radial velocity  $u(z,r)$  is given by Eq 3. It implies a parabolic profile without slip at the adjacent surfaces,

i.e.  $u(z,r) = 0$  at  $z = 0$  and  $\xi$ .  $u(z,r)$  will be greatest half-way between the surfaces. Fluid will be pulled towards the middle by the viscosity. The volumetric flow rate across a cylindrical surface at  $r$  is represented by Eq. 4,

$$u(z,r) = z (\hat{1}-z) \phi(r) \tag{3}$$

$$Q = \int_0^\xi u(z,r) 2\pi r dz \tag{4}$$

Further, by equating the change in volumetric flow rate to the volume of liquid displaced by the approaching surface in unit time,

$$dQ = 2 \delta r \delta z V \tag{5}$$

$$\phi(r) = 3rV/\xi^3 \tag{6}$$

Now, equating mechanical work to the energy dissipated due to viscosity,

$$FV = \int_0^\xi (\partial u/\partial z) 2 \delta r \delta z \tag{7}$$

$$FV = \int_0^\xi \int_0^r \tau \frac{\partial u}{\partial z} 2\pi r dr dz \tag{8}$$

Substituting for  $\partial u/\partial z$  and integrating with respect to  $z$  yields the relation

$$V = \frac{-dh}{dt} = \frac{F}{6\pi\mu \int_0^r \frac{r^3}{\xi^3} dr} \tag{9}$$

When approaching surface is flat disc of radius  $c$ , i.e.  $\xi = \text{constant} = h$

Time required for the thinning of the film from thickness  $h_1$  to  $h_2$  is,

$$t_{1,2} = \frac{\mu\Delta\rho g b^5}{4\sigma^2} \left[ \frac{1}{h_2^2} - \frac{1}{h_1^2} \right] \tag{10}$$

Assumptions involved in obtaining Eq 10 are as following, a) Liquid drop of radius  $b$  approaches a flat interface under its own weight. b) Drop undergoes a small deformation. Film does not drain regularly and it may rupture before drainage is complete, resulting in a distribution of coalescence times.

### Observations and Predictions

Time of fall of drop of distill water through organic phase towards the two phase interface has been observed and presented in Figure 2. With increase in the concentration of TBP, time of fall of drop towards the phase interface increases. This is because of increased density and the viscosity of the organic surrounding the drop. In presence of emulsifier SPAN 80 (3 % v/v), time of fall has larger values as shown in

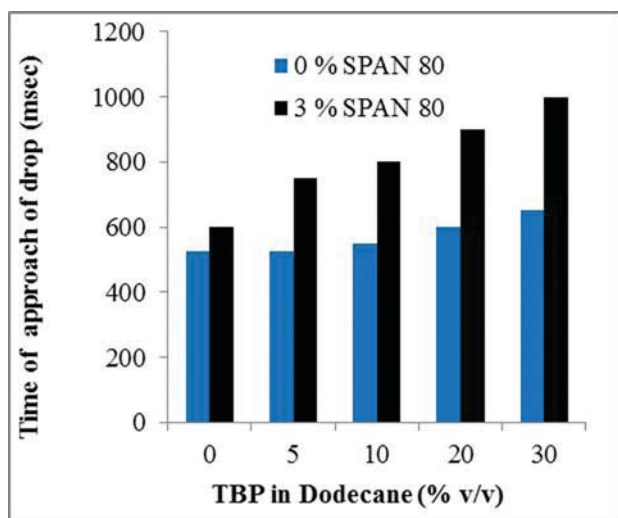


Fig. 2: Time of approach of drop to interface

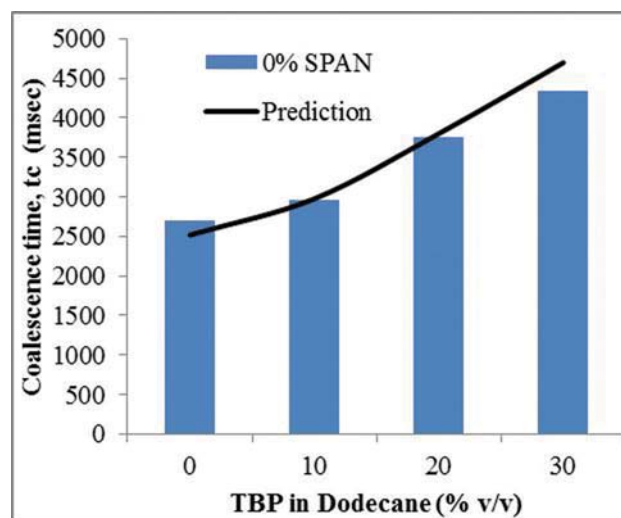


Fig. 3: Coalescence time of drop

Figure 2. This is because of further rise in the density and viscosity of the continuous phase with the emulsifier. Approach velocity of drop,  $u_t$ , towards the two phase interface has been found to be in between Stokes and Newton’s law regime through  $K$  values ( $K = D_p \{ \rho (\rho_p - \rho) / \eta^2 \}^{1/3}$ ). Density and viscosity have been estimated through densimeter and viscometer for varying composition of solutions. Emulsification carried out in laboratory at a speed of 3000 RPM, leads to drop diameter of dispersed phase of the order of 1 mm. Accordingly, spherical drop of 1 microlitre volume has been taken for  $D_p$  as  $0.124e-02$  m.  $u_t$  has been calculated through Equation 11 using a value of  $C_D$  found by trial, shown in Table 1.

Table 1: Theoretical values of approach velocity of drop towards the Interface

TBP in dodecane v/v	$C_D$	$u_t$ m/s	$Re_{p,cal}$	$Re_{p,theoretical}$
0%	1.85	0.04955	34.775	34.8
5%	1.85	0.04817	34.217	34.8
10%	2	0.04497	30.772	30
20%	2.32	0.03924	25.231	25.4
30%	2.5	0.03533	22.26	22.5

$$u_t = \{ (4 D_p g (\rho_p - \rho)) / 3 C_D \rho \}^{1/2} \tag{11}$$

Through  $u_t$ , time of approach of drop to interface has been evaluated and shown in Table 2 with the experimental data. Distance of travel for the drop is taken as  $3.75e-02$  m. Time for coalescence of drop of distilled water to its bulk phase has been observed and presented in Figure 3. With gradual increase in concentration of TBP, coalescence time also increases. This is because of the increase in viscosity of organic and decrease in its interfacial tension with the increase in TBP concentration. Theoretical values for the

coalescence time (shown in Figure 3 along with the data) have been estimated through Equation 10 using physical properties of solutions and film thicknesses according to Ghosh and Juvekar. Interfacial tension of solutions has been measured using spinning drop tensiometer.

Table 2: Time of approach of drop to interface

TBP % v/v	$u_t$ m/s	Time (Data)	Time (Eq 11)
0%	0.04955	600 ms	756.81 ms
5%	0.04817	750 ms	778.49 ms
10%	0.04497	800 ms	833.89 ms
20%	0.03924	900 ms	955.66 ms
30%	0.03533	1000 ms	1061.42 ms

It has been observed that with presence of emulsifier in organic phase (3 % SPAN v/v), coalescence time are two orders of magnitude higher than the coalescence time when no emulsifier present. This is because of one order of magnitude reduction of interfacial tension when emulsifier is present in the organic phase. Further, it has been observed that presence of emulsifier leads to decrease in coalescence time with increase in concentration of TBP. This is due to the increase in interfacial tension with increasing TBP in presence of emulsifier. Theoretical values are found to be in agreement with the data. The small deviations between predicted and observed values are expected to reduce further if the effect of the approach velocity of drop is accounted in the mathematical model.

### Conclusions

Coalescence time has been found virtually one order of magnitude greater than the time of approach of

drop towards the interface for the present organic pool length. Presence of emulsifier leads to higher approach and coalescence time due to increase in the viscosity of continuous phase and reduction in interfacial tension. Time of approach of drop towards the interface also rises with the increase in the concentration of the TBP, which is more prominent in presence of emulsifier. Increasing TBP concentration in presence of emulsifier, leads to decrease in coalescence time. The study will be helpful in online characterization of dispersion stability and coalescence during a liquid liquid extraction process.

### References

1. Charles, G. E., Mason, S. G. "The coalescence of liquid drops with flat liquid/liquid interfaces". *Journal of Colloid Science*, 15, (1960): 236-267.
2. Gillespie, T., Rideal, E. K. "The coalescence of drops at an oil-water interface". *Transactions of the Faraday Society*, 52, (1956): 173-183.
3. Reynolds, O. "On the theory of lubrication and its application to Mr. Beauchamp's towers experiments". *Phil. Trans. R. Soc. Lond.*, 177, (1886): 157.
4. Ghosh, P., Juvekar, V. A. "Analysis of the drop-rest phenomenon". *Trans IChemE*, 80, (2002): 715-728.

# Proton Beam Set-up for Radiobiological Studies

N.N. Bhat and B.K. Sapra

<sup>1</sup>Radiological Physics and Advisory Division

and

S.K. Gupta

Ion Accelerator Development Division

## Abstract

Radiobiological effects are known to vary with physical modifying factors such as linear energy transfer, type of radiation, fractionated and protracted irradiation. An irradiation setup has been established for exploring efficacy of low energy proton beam and to explore the physical modifying factors. Various beam line components were designed and fabricated indigenously. Beam parameters were optimized for the planned R&D projects and extensive studies were conducted to establish efficacy of proton beam.

## Introduction

Biological response towards various type of radiation depends largely on type of interaction and the way energy is deposited in the media. It is intriguing to explore these interactions using energetic charged particles as probes. Increasingly, these densely ionizing charged particles are being used in cancer therapy applications. In addition, we find their presence in space applications, accelerator projects used for scientific applications and many more. It is also interesting to note that neutron, though an uncharged particle, its mode of interaction is predominantly through knocking out protons from hydrogenous biological systems; and these protons being charged light ions having low energies, produce very dense ionization in media capable of creating biological lesions.

Unlike gamma irradiation facilities as well as other common radiations used in radiobiological studies such as X-rays and electron beams, charged particle irradiation setups are not fairly simple. In BARC, using Folded Tandem Ion Accelerator (FOTIA) at Ion

Accelerator Development Division (IADD), a proton beam facility has been setup for radiobiological studies. This setup has facilitated irradiation of model cellular systems such as cultured mammalian cells, yeast cells and bacterial cells.

## The layout

The schematic layout of the facility is shown in Fig. 1. The primary beam from FOTIA was diffused using a thin gold foil placed on a movable ladder inside a general purpose scattering chamber. The diffused proton beam was channelled using a long drift tube. At the end of the drift tube, diffused proton beam was taken out into atmospheric conditions through a thin titanium foil window which helped to isolate the vacuum of the beam line. Cell samples to be irradiated are mounted on petri plates. These plates were placed on the window with mounts specially designed for the purpose. The sample holder helped to reproduce the geometry of irradiation and easy changing of samples.

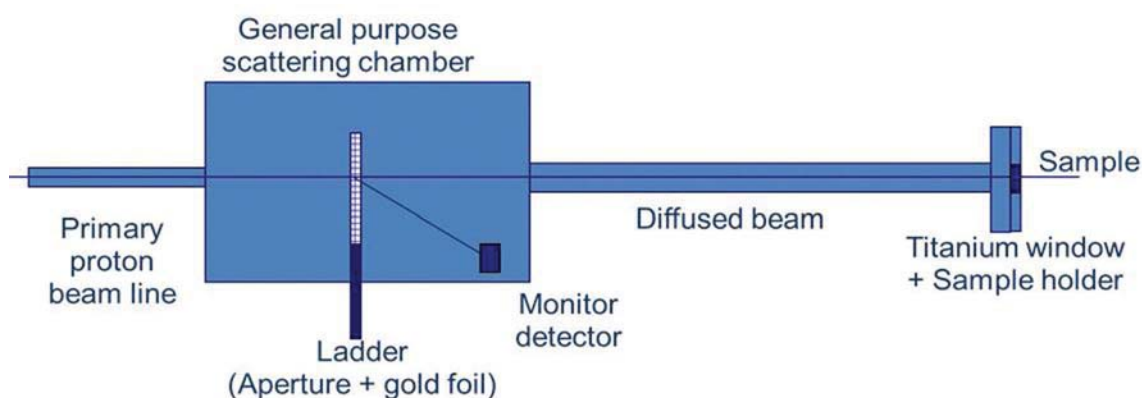


Fig.1: Schematic layout of proton beam setup for radiobiology experiments

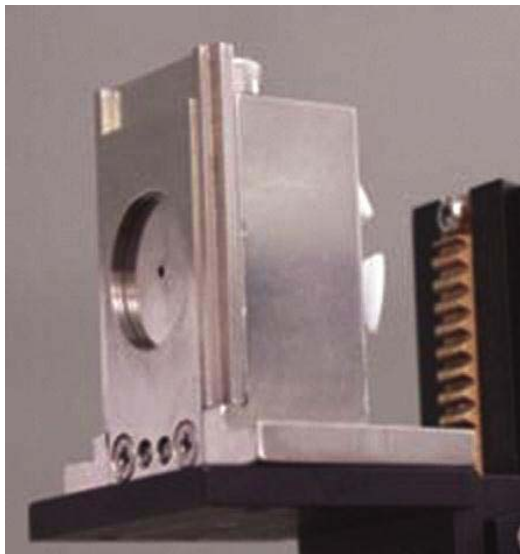


Fig. 2: SSB Detector mount used for fluence calibration

**Sample preparation**

Extensive optimization has been carried out to prepare cellular targets using various model cellular systems. For mammalian cells which grow on the surface with monolayer spread, the cells were grown on standard culture plates. These plates were mounted on the specially designed sample holder and positioned against the titanium window for irradiation. For suspension cultures and non-adhering cells such as human peripheral blood lymphocytes, yeast cells and bacterial cells, the cells were spread on 0.2 μm filter paper. This was done by passing the cell suspension through the paper by vacuum filtration. By this process, cells get spread on the filter paper in near mono layer geometry. The filter paper was mounted on a petri plate for irradiation.

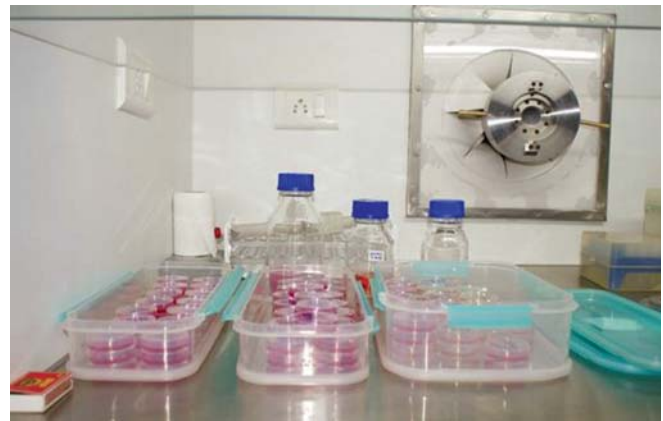
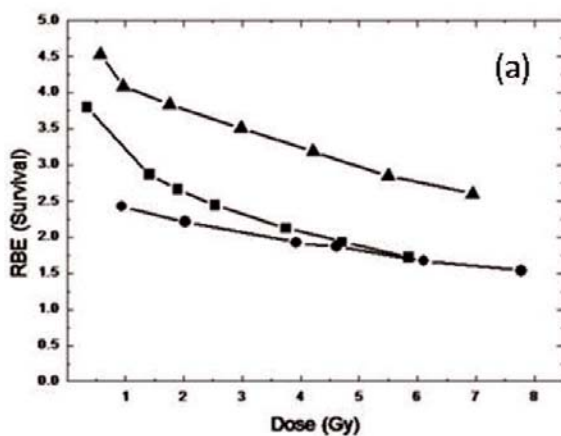


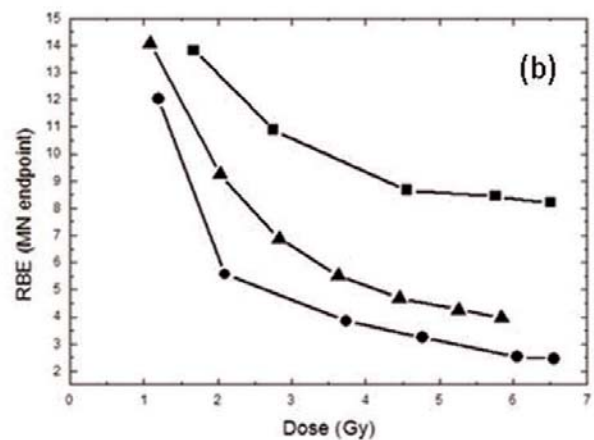
Fig. 3: Laminar hood housing titanium window for proton beam irradiation

**Calibration of set-up**

Two silicon surface barrier (SSB) detectors (M1 and M2) kept at an angle from the primary beam have helped to detect the scattered beam. One more detector (S) was placed at the titanium window simulating the geometry of samples to calibrate the fluence. The ratio between M1+M2 and S was estimated by repeated trials. The detector S was provided with calibrated collimator to reduce the count rate and dead time of the detector as shown in Fig 2. The detector S was replaced with sample for irradiation. The fluence to the sample was monitored with the M1 and M2 detectors with the help of pre-established ratio. The dose was calculated using SRIM software which has helped to estimate the linear energy transfer in the cellular medium. The uniformity of the beam was checked by scanning the collimated S detector mounted on an X-Y scanner.



(●) CHO cells (■) A549 cells (▲) MCF-7 cells



(●) CHO cells (■) A549 cells (▲) MCF-7

Fig. 4: (a) Variation of RBE for survival curve (b) Variation of RBE for micronucleus induction

## Irradiation with proton beam

The titanium beam window is housed in a laminar hood as shown in Fig 3, for aseptic handling of cell samples, which is a requirement in radiobiology experiments. The laminar hood also helped in preparation of samples. Since low energy protons cannot penetrate thick medium above the cells, during irradiation, media was briefly taken out by aspiration and cells mounted for irradiation. Duration of irradiation is typically about 1-2 minutes. Cells were supplemented with culture media quickly after the irradiation.

## Studies conducted

Many studies were conducted using radiobiological endpoints such as cell killing, chromosomal aberrations, micronucleus induction, premature chromosome condensation, gamma H2AX, gene expressions, etc., and interesting results were obtained. Relative Biological Effectiveness (RBE) in the range of 1.4-14 was estimated for these endpoints. Variation of RBE for Survival and micronucleus induction as representative indicators of biological damages and their comparison with gamma rays are shown in Fig 4(a&b).

## Conclusions

These results are useful for upcoming proton beam therapy applications, biomarker studies for high LET exposures and also to mechanistically explain effects of neutrons in the similar energies. The facility has opened up an opportunity to explore effects of high LET proton beam on model cellular systems which demand atmospheric conditions with stringent requirement of aseptically clean setup.

## References

1. Rajesha K. Nairy, N. N. Bhat, Anjaria K. B., Utkarsha Desai, Usha Yadav, Rajesh Chaurasia, Kapil Shirsath, B.K. Sapra and Narayana Yerol, Relative Biological Effectiveness studies using 3 MeV Proton beam from Folded Tandem Ion Accelerator: An experimental and theoretical approach, *Physics in Medicine and Biology* (Communicated).
2. Himanshi Narang, Amit Kumar, N. N. Bhat, Badri N. Pandey, Anu Ghosh, Effect of Proton and Gamma Irradiation on Human Lung Carcinoma Cells: Gene Expression, Cell Cycle, Cell Death, Epithelial-Mesenchymal Transition and Cancer-Stem Cell trait as Biological End Points. *Mutation Research* 2015 Jul 26; 780:35-46.
3. Somnath Ghosh, N. N. Bhat, S. Santra, R. G. Thomas, S.K. Gupta, R.K. Choudhury and Malini Krishna. Low energy proton beam induces efficient cell killing in A549 lung adenocarcinoma cells. *Cancer Investigation*, 28:615-622 (2010)
4. Himanshi Narang, N. N. Bhat, S. K. Gupta, S Santra, R. K. Choudhary, S. Kailash and Malini Krishna. Differential activation of mitogen-activated protein kinases following high and low LET radiation in murine macrophage cell line, *Mol. Cell Biochem* Apr;324(1-2):85-91. (2009)
5. Himanshi Narang, N. N. Bhat, S. K. Gupta, S Santra, R. K. Choudhary, S. Kailash and Malini Krishna. Differential activation of mitogen-activated protein kinases following high and low LET radiation in murine macrophage cell line, *Mol. Cell Biochem* Apr;324(1-2):85-91. (2009)

# High Temperature Deformation Behavior of Nb-1Zr and Nb-1Zr-0.1C

R. Kapoor, A.N. Behera, A. Sarkar and J.K. Chakravartty  
Materials Group

## Abstract

*Nb-1Zr-0.1C alloy is a potential candidate material for use in advanced nuclear reactors. An essential step in the fabrication of components is the thermo-mechanical processing of the alloy. These are performed at high temperatures, where either dynamic recovery or dynamic recrystallization occurs. The resultant microstructure is either refined or coarsened depending upon the applied strain rates and temperatures of hot working. Here the microstructural evolution of hot deformed Nb-1Zr and Nb-1Zr-0.1C alloys are presented and optimum domains of their hot working are identified. The microstructural features of dynamic recovery and recrystallization obtained during hot deformation are correlated to the corresponding stress-strain behaviour and strain rate sensitivity.*

## Introduction

Niobium alloys (melting point of  $\sim 2460$  °C) offer attractive high-temperature properties suitable for applications in nuclear environments including high temperature strength, good thermal conductivity and compatibility with most liquid metal coolants [1-4]. Nb alloyed with 1%Zr adds to solid solution hardening and the addition of 0.1 wt% C results in very fine (Nb,Zr)C precipitates which enhances creep resistance [5]. Due to these properties, Nb-Zr alloys are being actively considered for use in high temperature applications in compact high temperature reactor (CHTR) [6]. Fabrication of these alloys into products with desired microstructure and free of volumetric defects requires optimum thermo-mechanical processing.

The usual route during industrial processing of materials is melting, casting, thermo-mechanical processing, and secondary processing steps like intermediate heat treatment, cold working, finishing operations, etc., resulting in the final product. Of these, thermo-mechanical processing is an important step where the cast microstructure breaks down and an intermediate defect free microstructure evolves. Thermo-mechanical processing (TMP) is carried out at high temperatures (usually around half the melting point and is also referred to as hot condition) with the material being deformed to large strains either in single or multiple steps. The two important independent parameters during TMP are the temperature ( $T$ ) and strain rate ( $\dot{\epsilon}$ ) of deformation. Microstructural evolution during thermo-mechanical processing is dependent on the restoration mechanisms operating during those processing conditions, such as dynamic recovery, dynamic

recrystallization and grain boundary deformation. Of these dynamic recrystallization (DRX) is an important restoration mechanism observed in almost all hot deformed metals and alloys. An overview of the hot deformation mechanisms can be found in References [7] and [8]. Presented here is the hot deformation behaviour and microstructural evolution of Nb-1Zr and Nb-1Zr-0.1C alloy deformed at temperatures from 700 to 1700 °C and strain rates of  $3 \times 10^{-3}$  to  $1 \text{ s}^{-1}$ . The basics of the method to determine the optimum hot working parameters are also discussed.

## Determining the optimum hot workability

The optimum hot working conditions ( $T$  and  $\dot{\epsilon}$ ) are determined on a lab scale by carrying out compression tests over a range of temperatures and strain rates. Apart from flow stress ( $\sigma$ ) being of prime concern during deformation (lower flow stresses imply easier deformation), the strain rate sensitivity is also important in determining the optimum hot working domain. The strain rate sensitivity  $m$  is the slope of the  $\log \sigma$  vs.  $\log \dot{\epsilon}$  curve, i.e.

$$m = \frac{\partial \log \sigma}{\partial \log \dot{\epsilon}} \quad (1)$$

A higher value of strain rate sensitivity ensures strain rate hardening, which delays necking in tension [9, 10] and prevents instabilities in compression [11]. The method of determining and mapping out  $m$  is shown in Fig. 1. The strain rate sensitivity is calculated from the  $\sigma$ - $\dot{\epsilon}$  data at large strain values (usually between 0.5 to 0.6) for various  $T$  and  $\dot{\epsilon}$  as shown in Fig. 1(a) and (b). For each strain rate employed, the stress values

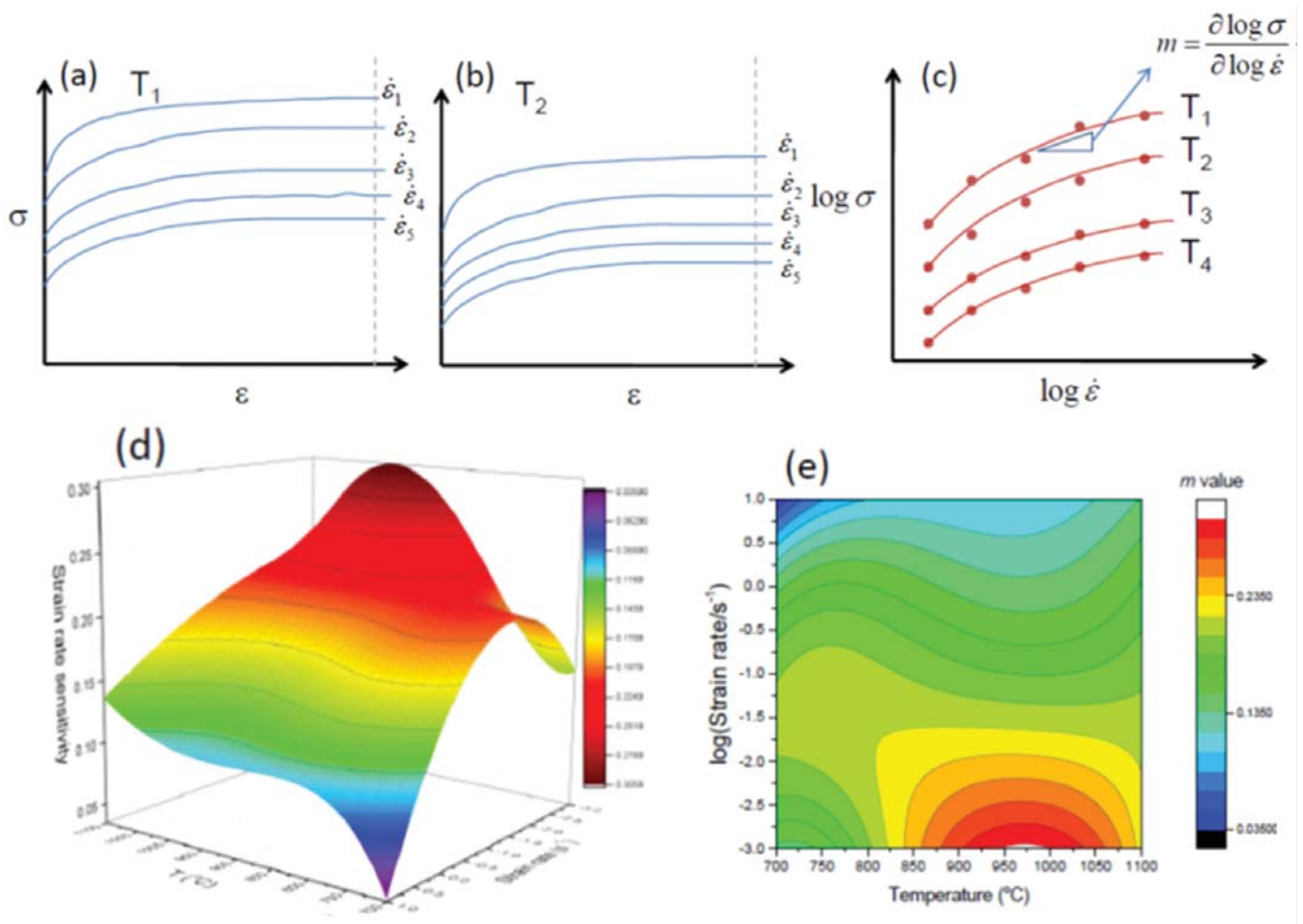


Fig. 1: Sequence of determining the strain rate sensitivity map from compression tests. (a) Stress – strain curves at a given temperature (a)  $T_1$  and (b)  $T_2$  for different strain rates. (c) Log stress vs. log strain rate fitted to a cubic polynomial, the slope of which is  $m$ . (d) the 3 dimensional plot of  $m$  vs.  $T$  and  $\log \dot{\epsilon}$ . (e) the corresponding contour plot

are interpolated at finely spaced  $\log \sigma$  and  $1/T$  intervals. At each of the temperature values (including interpolated ones) the  $\log \sigma$  vs.  $\log \dot{\epsilon}$  data is fitted to a cubic polynomial as seen in Fig. 3(c) and the stress values interpolated at finely spaced  $\log \dot{\epsilon}$  values. These two interpolations produce a grid of stress values over the entire strain rate and temperature range of tests. The strain rate sensitivity is calculated by taking the derivative at each point of the  $\log \sigma$  -  $\log \dot{\epsilon}$  curve (eq.1). These calculated values of  $m$  are plotted for each grid point on the  $T$  and  $\log \dot{\epsilon}$  space resulting in a 3D plot seen in Fig. 1(d). This is then translated into a 2-D contour map as shown in Fig. 1(e). Such maps show domains of high  $m$  (as shown in red) and regions of low  $m$  (as shown in blue). The contours join points of equal  $m$  values, making them iso-strain rate sensitivity contours. The microstructure at different conditions of temperature and strain rate are then observed and correlated with the flow stress and strain rate sensitivity. There are numerous such studies where the strain rate sensitivity is computed and plotted as a contour map (e.g., [12-15]). Apart from

identifying regimes of high  $m$ , regimes of instability and flow localization also need to be identified and avoided during processing. In literature there are several approaches for identification of regimes of instability during deformation, based on work-hardening/softening [11] and extremum principles [16]. However, a conservative condition for the occurrence of instability in these methods is that the value of  $m$  reduces to  $m < 0$ . There are other less stringent conditions for instability, but some of these are controversial and will not be discussed here. As an example Ref. [15] discusses these instability conditions for the specific case of cast Zr-2.5Nb.

### Hot deformation of Nb-1Zr and Nb-1Zr0.1C

The hot deformation behaviour and microstructural evolution of Nb-1Zr and Nb-1Zr-0.1C were studied using compression tests carried out in vacuum to a true strain of 0.6 in the temperature range of 700 to 1700 °C and the strain rate range of  $10^{-3}$  to  $10$  s $^{-1}$ . The flow stress of Nb-1Zr-0.1C was higher than that of Nb-1Zr as seen in Fig. 2 for two strain rates of 0.1

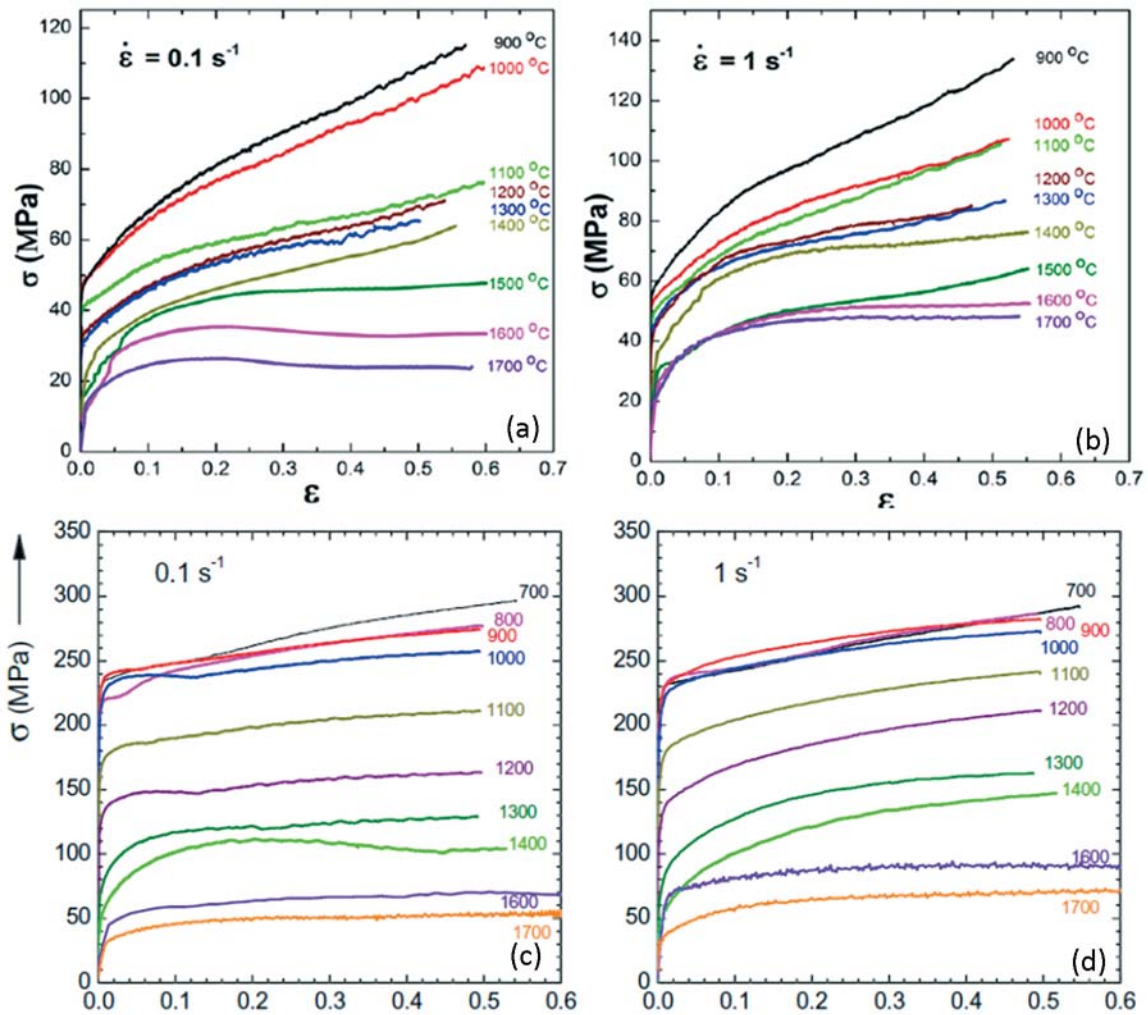


Fig. 2: True stress vs. true strain of Nb-1Zr-0.1C (a) and (b), and Nb-1Zr (c) and (d), at strain rates and temperatures as mentioned

and  $1 \text{ s}^{-1}$ . For example, at  $1000 \text{ °C}$  and  $1 \text{ s}^{-1}$ , Nb-1Zr-0.1C had a flow stress of 250 MPa with moderate strain-hardening, whereas Nb-1Zr for the same condition showed a low yield stress and a substantial work-hardening but to lower stress values. At higher temperatures between 1500 to 1700 °C, both alloys showed steady state behaviour but the flow stress of Nb-1Zr-0.1C was still higher than that of Nb-1Zr.

The high strain rate sensitivity domain of Nb-1Zr occurred at lower temperature ( $1500 \text{ °C}$ ) as compared to that of Nb-1Zr-0.1C ( $1700 \text{ °C}$ ) as seen in Fig. 3. Nb-1Zr-0.1C showed a high  $m$  domain from 1500 to 1700 °C and  $3 \times 10^{-3}$  to  $0.1 \text{ s}^{-1}$ , whereas Nb-1Zr showed it in the range from

1300 to 1500 °C and  $10^{-2}$  to  $1 \text{ s}^{-1}$ . Addition of carbon to Nb-1Zr is known to result in formation of (Nb,Zr)C which is a stable phase. This carbide formation shifts the high  $m$  domain to higher temperatures. For both

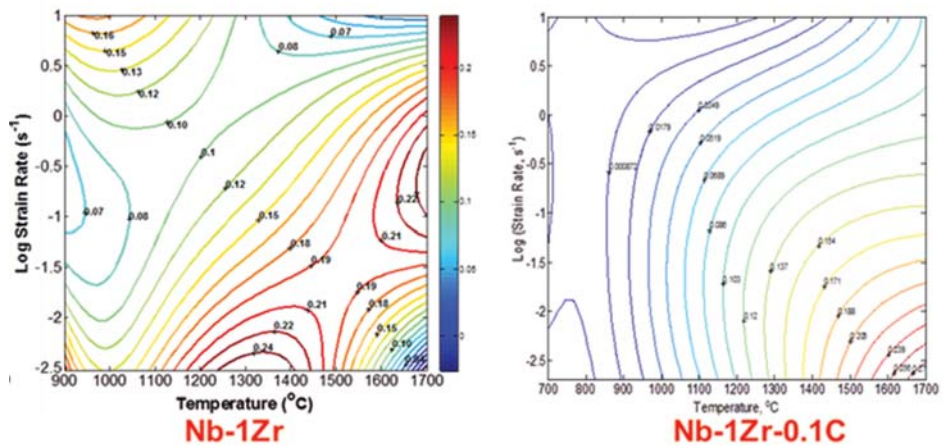
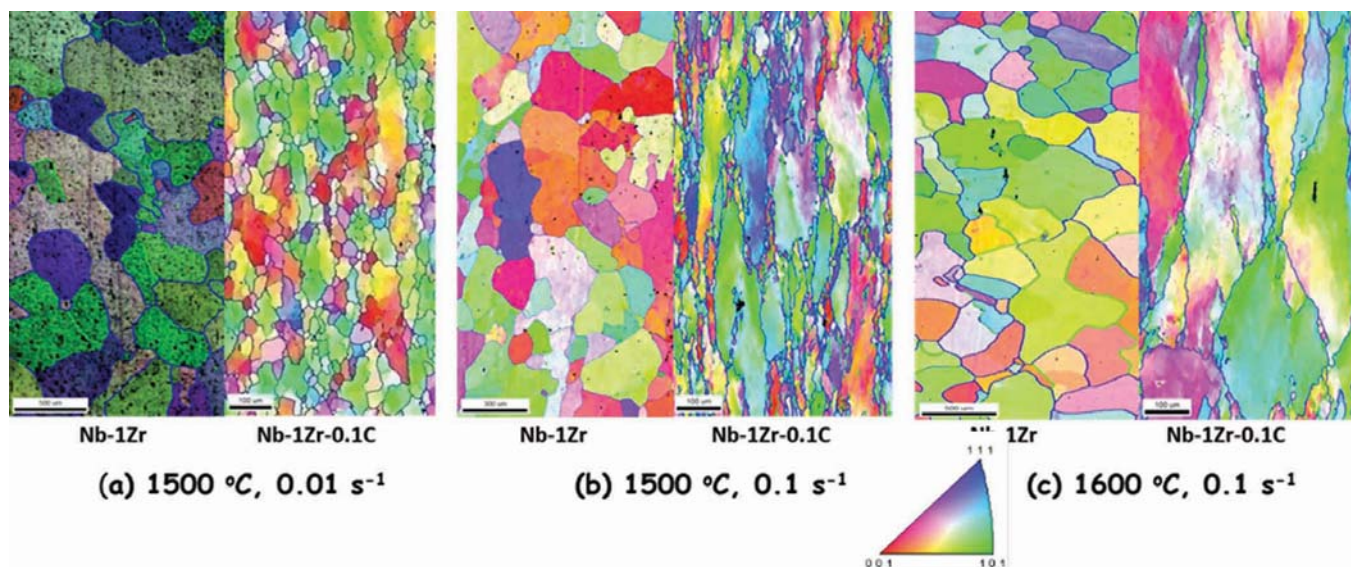


Fig. 3: Iso-strain rate sensitivity contour maps of Nb-1Zr and Nb-1Zr-0.1C



**Fig. 4:** EBSD maps of Nb-1Zr and Nb-1Zr-0.1C deformed at 1500 °C 0.01 and 0.1 s<sup>-1</sup> and 1600 °C and 0.1 s<sup>-1</sup> up to a strain of 0.6. The colours represent the crystal orientation according to stereographic triangle with respect to normal of polishing surface

alloys, the low strain rate sensitivity domain appeared at lower temperatures and higher strain rates.

**Microstructural comparison**

Fig. 4 shows a comparison of electron back scatter diffraction (EBSD) maps of Nb-1Zr and Nb-1Zr-0.1C alloys deformed respectively at temperature of 1500 °C for strain rates of 0.01 and 0.1 s<sup>-1</sup> and at 1600 °C for strain rate of 0.1 s<sup>-1</sup>. For both alloys, at strain rate of 0.01 s<sup>-1</sup> and temperature of 1500 °C grains appeared recrystallized and nearly equiaxed. At this condition, grains of Nb-0.1Zr-0.1C are finer as compared to that of Nb-1Zr alloy. For strain rate of 0.1 s<sup>-1</sup> at 1500 °C Nb-1Zr-0.1C showed elongated grains whereas Nb-1Zr showed equiaxed grains. At this condition dynamic recrystallization appeared to have started but remained incomplete for Nb-1Zr-0.1C alloys whereas it appeared completed for Nb-1Zr. At strain rate of 0.1 s<sup>-1</sup> DRX microstructure results from the initial grains which get elongated during deformation for Nb-1Zr-0.1C alloys at 1500 and 1600 °C. Decreasing temperature and increasing strain rate resulted in grain refinement.

**Effect of carbon addition**

The role of zirconium and carbon in Nb is to strengthen the material through solid solution and precipitation, respectively. The stress - strain rate data at 900 and 1000 °C of Nb [17], Nb-1Zr and Nb-1Zr-0.1C [14] is shown in Fig. 5. It is seen that Nb and Nb-1Zr lie in the same stress range and lower to that of Nb-1Zr-0.1C. This shows that the solid solution effect of Zr is insignificant as compared to that hardening produced by carbide precipitates. The activation

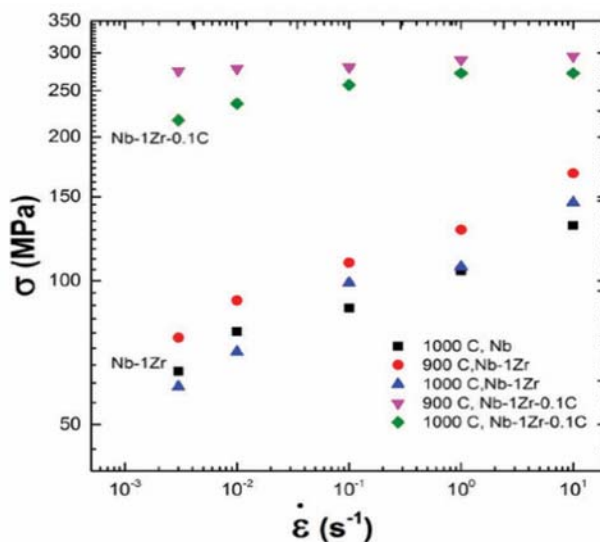


**Fig. 5:** Flow stress vs. strain rate for Nb [17], Nb-1Zr and Nb-1Zr-0.1C [14]

energies for the deformation of Nb and Nb-1Zr alloys are 245 and 260 kJ/mol respectively, while that of Nb-1Zr-0.1C is 360 kJ/mol. A higher activation energy suggests that for same conditions the deformation is more difficult. Further, as the activation energy for self-diffusion of Nb is 400 kJ/mol, it implies that for Nb and Nb-1Zr ( $Q < Q_{SD}$ ) dislocation based core diffusion may be the rate controlling mechanism.

**Conclusions**

A comparison of the hot deformation behaviour of Nb-1Zr and Nb-1Zr-0.1C showed the following.

1. Nb-1Zr-0.1C shows a higher flow stress as compared to Nb-1Zr.
2. Both Nb-1Zr and Nb-1Zr-0.1C dynamically recrystallizes during hot deformation.

3. The temperature of dynamic recrystallization of Nb-1Zr is lower as compared to Nb-1Zr-0.1C (1300 to 1500 °C vs. 1500 to 1700 °C).
4. Nb-1Zr showed equiaxed grains indicative of a completed dynamic recrystallization process whereas Nb-1Zr-0.1C showed elongated grains with fine grains at grain boundaries (necklace structure) indicative of start but incomplete dynamic recrystallization process.

## References

1. J.R. Distefano, *Journal of Materials Engineering*, 11 (1989) 215-225.
2. S.J. Zinkle, L.J. Ott, D.T. Ingersoll, R.J. Ellis, M.L. Grossbeck, *AIP Conference Proceedings*, 608 (2002), 1063-1073.
3. R.E. Gold, D.L. Harrod, *Journal of Nuclear Materials*, 85-86 (1979) 805-815.
4. D.J. Mazey, C.A. English, *Journal of the Less Common Metals*, 100 (1984) 385-427.
5. E.J. Delgrosso, C.E. Carlson, J.J. Kaminsky, *Journal of the Less Common Metals*, 12 (1967) 173-201.
6. I.V. Dulera, R.K. Sinha, *Journal of Nuclear Materials*, 383 (2008) 183-188.
7. D.L. Bourell, H.J. McQueen, *Journal of Materials Shaping Technology*, 5 (1987) 163-189.
8. H.J. McQueen and D.L. Bourell, *Journal of Materials Shaping Technology*, 5 (1988) 53-73.
9. E.W. Hart, *Acta Metallurgica*, 15 (1967) 351-355.
10. J.D. Campbell, *Journal of Mechanics and Physics of Solids*, 15 (1967) 359-370.
11. J.J. Jonas, R.A. Holt, C.E. Coleman, *Acta Metallurgica*, 24 (1976) 911-918.
12. R. Kapoor, J.K. Chakravartty, *Journal of Nuclear Materials*, 306 (2002) 126-133.
13. J.K. Chakravartty, R. Kapoor, S. Banerjee, Y.V.R.K. Prasad, *Journal of Nuclear Materials*, 362 (2007) 75-86.
14. A. Sarkar, R. Kapoor, A. Verma, J.K. Chakravartty, A.K. Suri, *Journal of Nuclear Materials*, 422 (2012) 1-7.
15. J. K. Chakravartty, R. Kapoor, A. Sarkar, V. Kumar, S. K. Jha, N. Saibaba, and S. Banerjee, ASTM-STP1543, 2014, 17th International Symposium on Zirconium in the Nuclear Industry, [www.astm.org](http://www.astm.org) / doi: 10.1520/STP154320120197.
16. H. Zeigler, *Progress in Solid Mechanics*, vol. IV, I. N. Sneddon and R. Hill, Eds., North-Holland Publishing Company, Amsterdam, 1963, pp. 93-192.
17. A.N. Behera, R. Kapoor, A. Sarkar, J.K. Chakravartty, *Materials Science and Technology*, 30 (2014) 637-644.

# Development of Quick Scan Whole Body Monitor for *in-vivo* Monitoring of Radiation Workers and General Public

Rajesh Sankhla, I.S. Singh, D.D. Rao and K.S. Pradeepkumar  
Radiation Safety Systems Division

## Abstract

Whole Body monitoring of radiation workers at nuclear facilities is a regulatory requirement and is recommended for assessment of internal contamination due to gamma emitting radio nuclides. Additionally, nuclear accidents like Chernobyl, Fukushima and radiological accidents like Goiania have clearly highlighted the need for *in-vivo* monitoring of the members of the public during and/or after such accidents. To cater to these requirements, a high throughput, fast screening, standing linear geometry Quick Scan Whole Body Monitor (QS-WBM) is designed, fabricated and commissioned to measure internal contamination due to gamma emitting radio nuclides ( $E_{\gamma} > 200\text{keV}$ ) incorporated in the human body. The system is designed to achieve sensitivity comparable with conventional WBM for 1 - 2 minutes counting time and to accommodate different body sizes of Indian occupational workers. It is calibrated using BARC reference Bottle Mannequin Absorption (BOMAB) type phantom and also using a family of BOMAB type phantoms representative of different age groups namely 1-, 5-, 10-, 15- and 20- years. The developed system will also be highly useful during emergency situations when large numbers of persons are to be monitored in short interval of time.

**Keywords:** *in-vivo* monitoring, BOMAB phantom, WBM, calibration

## Introduction

The Quick Scan Whole Body Monitor (QS-WBM) is developed in response to the need of the DAE facilities for a whole body monitor that can quickly and efficiently monitor the radiation workers for internal contamination due to gamma emitting radio nuclides like fission and activation products during normal and emergency situations.

In the present scenario, a large number of radioactive sources are used in different industrial and medical applications. Accidents in handling of radioactive sources as well as the malevolent use of radiation must also be considered as a possible threat. In this kind of emergency situations, the personnel affected most likely, will be the members of the public in various age groups (child to adult). Although external dose to the public is of greater concern, there is also an evident need for rapid measurement of large groups of suspected internally contaminated people.

A conventional WBM is a scanning bed geometry Shadow Shield Whole Body Monitor (SSWBM) in which occupational workers are monitored for the detection of internal contamination due to gamma emitting radio nuclides. Scanning geometry is considered to be relatively accurate particularly for unknown distributions, as its response is nearly independent of the distribution of radionuclides in the body. However,

the scanning mode of counting requires 20 to 30 minutes whereas QS-WBM system has the capability to monitor an individual in ~one minute. This system has been fabricated indigenously and is therefore, cost effective. The QS-WBM follows the concept of shadow shield technique in which no gamma ray photon from background can reach directly to the open face of the detector without passing through the shield or after scattering through an angle greater than  $90^{\circ}$ .

The variation in physical sizes of subjects is known to introduce systematic error in the calibration of *in-vivo* monitors. In view of this, the QS-WBM is calibrated using a BARC reference BOMAB phantom and a family of BOMAB phantoms representative of the Indian population of different age groups. This article describes the criteria used for designing the QS-WBM, detailed information on its fabrication and calibration with BARC reference and family of BOMAB phantoms for high energy photons emitters ( $E_{\gamma} > 200\text{keV}$ ).

## Materials and Methods

### *Design aspects of the system*

The QS-WBM consists of three sided shielded cavity (50 mm lead) of outer dimensions 2170 mm(H) x 1225 mm(W) x 625 mm(D) and shielded detector mounting wall of outer dimensions 2170 mm(H)x 350 mm(W) x 215 mm(D). The system is designed to

achieve good sensitivity for 1- 5 minute counting time. It has no moving parts, has user-friendly operation and low maintenance and covers nearly 99% of the body sizes (child to adult height 75 cm to 180 cm and weight 9 kg to 66 kg ). The cavity size was optimized based on, the weight and height data of nearly 2000 occupational (radiation) workers. In order to accommodate almost all occupational workers and placement of the detectors, the internal height of the subject cavity was fixed at 190 cm. The subject standing platform size was optimized to 95 cm x 45 cm taking into consideration of subject’s belly size, gap required for entry and exit of the subject from QS-WBM. The shield thickness was optimized to 50 mm of lead, which provides nearly 4 Half Value Layer (HVL) for <sup>40</sup>K (1460 keV) gamma energy. The standing linear geometry WBM is incorporated with two NaI(Tl) detectors each of dimension 406 mm(L) x 127 mm(W) x 76 mm(D) for optimum measurement sensitivity. The detailed dimensions and design aspects of the system were provided to a private company for fabrication.

**Fabrication and installation of the system**

The fabrication of shielding enclosure for positioning the subject and shielding wall for detector was carried out using 50 mm thick lead inside a stainless steel (SS) frame. The outer cover of 3 mm thick stainless steel sheet was properly fastened to the frame. The structural frame is designed and fabricated using 5 mm thick SS angles, 3, 6, 10 and 20 mm thick SS plates. About 10 samples of SS plates and lead sheets were tested for radioactivity content prior to their use in the system to ensure that there are no detectable inherent primordial or anthropogenic sources

of radioactivity. The shield is constructed in a laminar fashion using 50 mm thick lead bricks and a total of 320 bricks of different sizes were assembled with interlocking arrangement from all the sides. Lead shield of nearly 4 Tons are used in detector and subject enclosure walls. All the shielded sides are divided into three independent compartments which provide excellent load sharing of nearly 2 m height of interlocked lead walls.

The assembled QS-WBM, occupies a floor space of 1230 cm x 90 cm and its height is ~ 217 cm. The exterior of the shield is aesthetically covered by 4 side panels of 2 mm thick powder coated mild steel sheet metal. The interior of the shield is also covered by 3 panels of 1 mm thick stainless steel sheet. The advantage of SS cover is that it can be easily cleaned and gives a comfortable feeling to the subject. The floor covers are replaceable in the event of contamination. The two NaI(Tl) detectors are configured vertically one below the other in a linear array on a common vertical axis and their placement was chosen based on anthropometric data of the



Fig.1: Shielded Cavity



Fig.2: Quick Scan WBM with subject

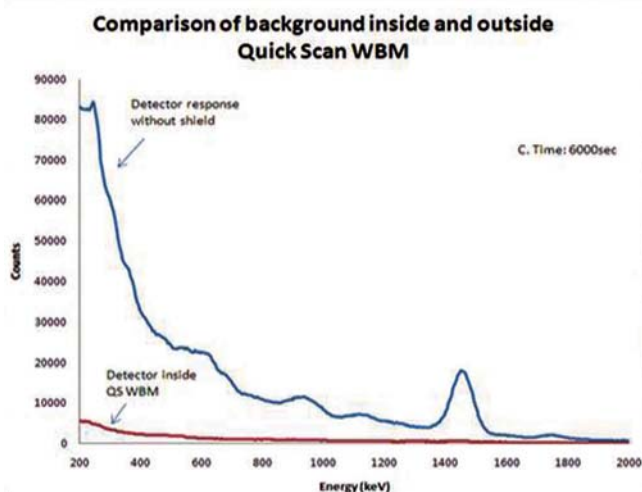
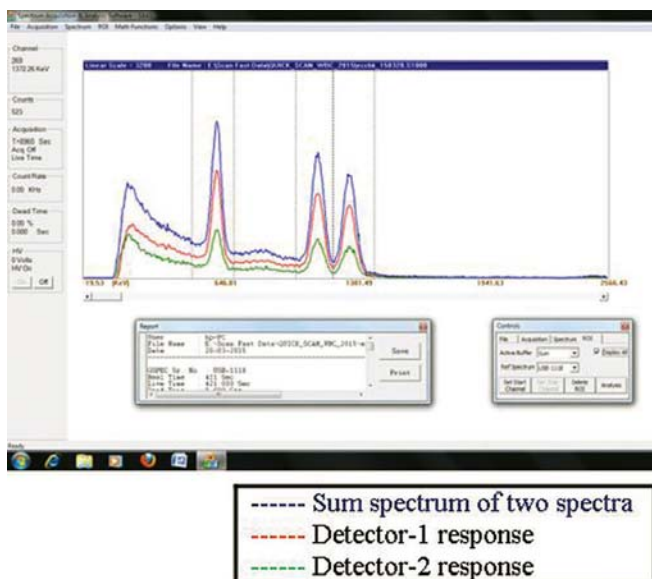


Fig.3: Comparison of background when detectors are inside and outside of QS-WBM

radiation workers. The subject can be reproducibly positioned at the centerline of the detectors by an indicator within the detector wall liner.

**Methodology for summing of gamma spectra of two NaI(Tl) detectors**

The two NaI(Tl) detectors placed vertically one below another are connected to two independent plug-on type 1K GSPEC Multi Channel Analyzer (MCAs, 1024 channel) so as to acquire the distinct spectra of each detector. The resolution of each detector is less than 8.5%. Use of two independent large size NaI(Tl) detectors provides higher efficiency for QS-WBM. The two detectors each of which views part of the body provide spectra separately and the output of both the detectors is required to be summed with respect to energy. A methodology was developed for summing of energy spectra of the two detectors and converting to single spectrum, which is used for analysis. This methodology is as follows (i) Energy calibration factors of both the MCAs are kept as close as possible by adjusting high voltage and amplifier gain (5keV/Channel). (ii) the energy calibration equation of either detector spectra is set as reference spectrum (user selectable).(iii) the first channel energy of reference spectrum is selected and the approximate closest energy channel from second spectrum is searched electronically and the contents of both the channels are added and stored as summed spectrum content of reference spectra energy. (iv) the sequence of operation of (iii) is continued till all 1024 channels of reference spectra are completed. (v) this algorithm is integrated into MCA gamma analysis software for enabling dynamic display of summed spectrum along



**Fig.4: Typical spectrum of QS-WBM**

with two spectra superimposed on one another. Figure-4 shows a screen shot of typical spectrum acquired in QS-WBM in which source is kept near to detector -1.

**Results and Discussions**

**Measurement of internal contamination**

As a common operational practice, daily energy calibration and acquisition of background spectra of the system for a given preset time is carried out. Subject data is collected in a standard personal data sheet which includes, name, designation, unit, TLD no., employee no., weight & height, routine/ special monitoring etc. After ensuring that there is no external contamination, subject is positioned on the platform inside the QS-WBM. The subject is monitored for given preset time and WBC software performs several functions such as stripping of background from subject spectra, estimation of body content for a given radionuclide, its intake and dose. Figure - 5 shows a typical spectrum of a subject with <sup>131</sup>I thyroidal content. The spectrum indicates <sup>131</sup>I peak only in the upper detector as nuclide is retained in thyroid and the standing position of the subject positions the neck in front of upper detector. The nature of individual detector spectrum, thus provides information on the localized contamination, if any.

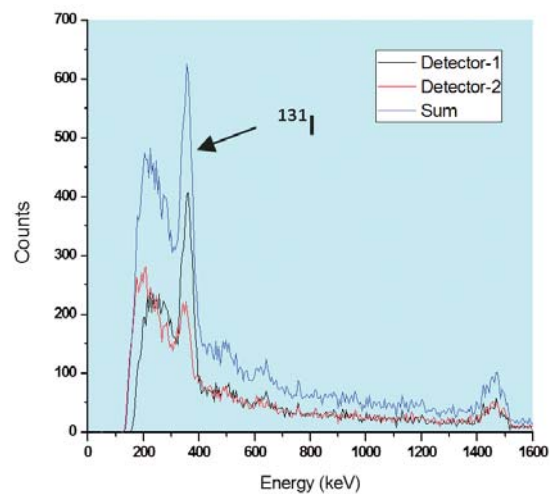
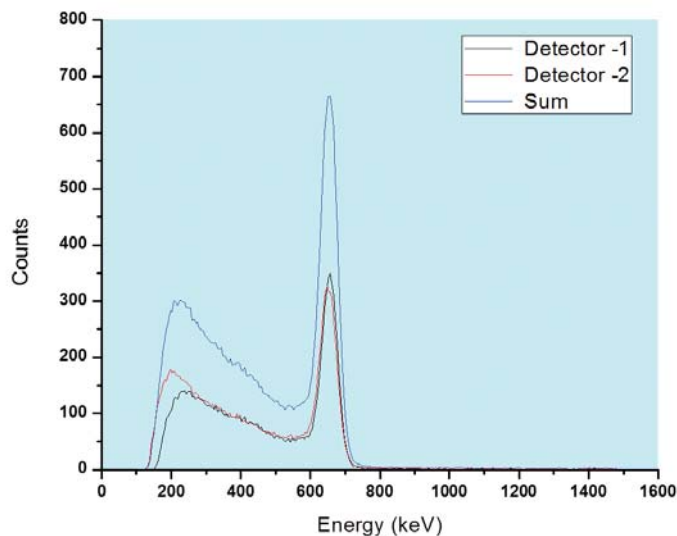
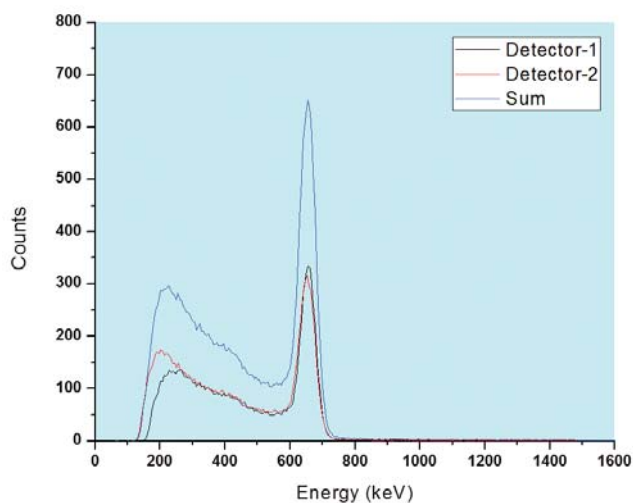


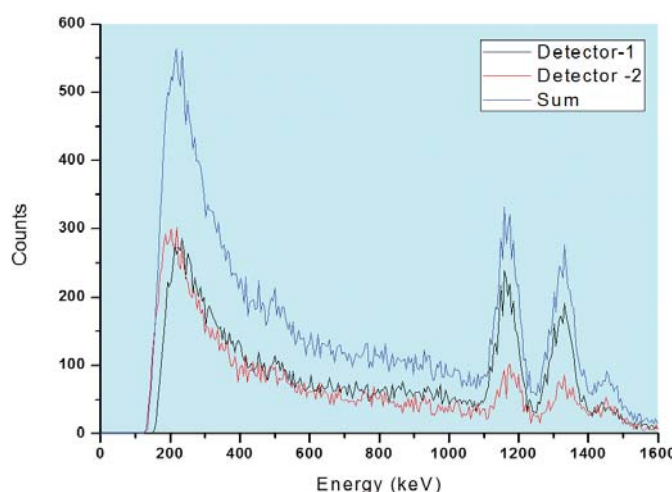
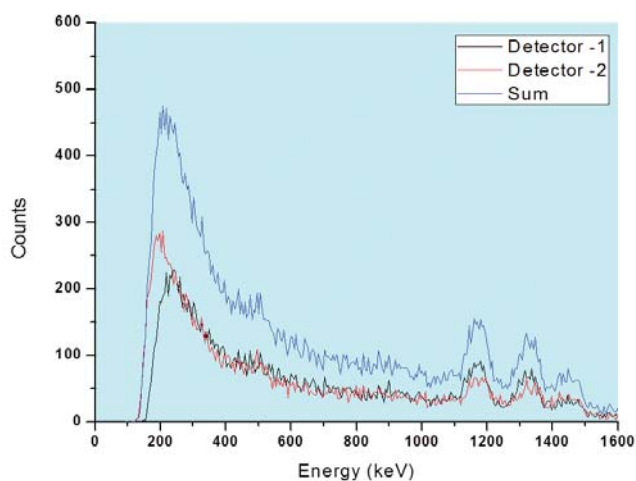
**Fig.5: Typical spectrum of a subject with <sup>131</sup>I**

**Identification of external contamination on subject**

The QS-WBM can be used to identify the external contamination (fixed) from the measured spectral characteristics of the worker. In such situations the subject is monitored in two positions: i) standing position – thorax facing the detector and ii) standing



**Figs. 6 & 7: Spectra of the front and rear portions of the phantom facing the detector when activity is distributed inside the phantom**



**Figs.8 & 9: Spectra of the front and rear portion of the subject facing the detector when external contamination is on the body of the subject**

position - vertebra facing the detector. The two spectra will be nearly identical if the contaminant is internal (Figure - 6 and 7). In case of external contamination the two spectra will not be identical and one of the detector spectra would have significantly higher photo peak area depending on the site of external contamination. For example, if the contamination is on the chest, hair, the spectra of position-1 would show significantly higher counts as compared to counting position-2. Figure- 8 and 9 gives the spectral characterization of two counting positions. This procedure is generally followed if the regular counting (position-1) gives significantly higher counts due to any given radionuclide.

**Calibration of QS-WBM**

In order to determine the amount of a radionuclide retained in the body, the detector response for known activity for a particular radionuclide in appropriate phantom is generated. This is carried out by placing known amount of activity of a radionuclide in suitable phantom and measuring the emitted photons to evaluate Calibration Factor (CF) in terms of cps/Bq.

**BOMAB phantom- BARC reference**

The Bottle Mannequin Absorption (BOMAB) phantom consists of ten containers of different shapes and volumes which represent Head, Neck, Thorax, Pelvis, Pair of Arms, Thighs and legs of a reference human body. The cross sections of the three blocks namely head, thorax and pelvis are elliptical while others are

**Table 1 : BARC reference BOMAB phantom parameters**

Phantom Part	Dimension (cm)	Length (cm)	% wrt total ht.	Weight (kg)	% wrt total wt.
Head	Major-18.4, Minor-14.0	19.6	11.8	4.2	6.4
Neck	Major-14.0, Minor-13.0	9.6	5.8	1.6	2.4
Thorax	Major-29.4, Minor-19.8	37.8	22.7	19.3	29.2
Pelvis	Major-35.2, Minor-19.8	19.4	11.7	11.5	17.4
Thigh	Major-15.4, Minor-14.2	39.8	24	5.7x2	17.3
Leg	Major-11.6, Minor-11.6	39.8	24	4.8x2	14.6
Arm	Major-9.2, Minor-9.2	56.4	34	4.2x2	12.7
		166 cm		66 kg	



**Fig.10: BARC reference BOMAB phantom**

circular in shape. Each container is fabricated from a light material- Poly Vinyl Chloride (PVC) of 3 mm thickness and is free from any leakage when filled with water. An inlet with a cap is provided at the top of each block for filling water in it. A 12 mm dia. PVC pipe is inserted and welded along the central axis of each block to facilitate placing of sealed sources for calibration. Each container is filled with water and when all the ten are assembled together, they approximate the physical shape of a human. Table– 1 shows the physical parameters of different parts of the phantom. This type of phantom is an IAEA approved type phantom and is in use at BARC and is suitable for the efficiency calibration of WBMs employed to measure internal contamination due to high energy photons (HEP) emitting radio nuclides.

**Family of BOMAB phantoms representative of male Indian population**

In general, the ICRP data on reference man for human tissues are employed for designing phantoms. However, these data are representative of Caucasian population. Recognizing that the Indians and other Asians differ considerably from the Caucasian in physique, National Nutrition Monitoring Board (NNMB) of Indian Council of Medical Research (ICMR) and further Dang et al.(1994), Jain et al.(1995) published data on physiological and anatomical parameters and provided guidance for working out the dimensions for a family of phantoms representing Indian population.

**Table 2: Physical parameters of different sections of the phantoms of Indian male subjects of different age groups. H=height, a= semi-major axis, b= semi-minor axis, V= volume and C= circumference of the block. Mehta et al. (2003)**

Age	Physical Parameters	Head	Neck	Thorax	Pelvis	Thigh	Leg	Arm	Total
1 week	H cm	6.4	4.1	12.8	9.8	8.5	8.5	12	51
	a cm	9.6	5.3	12.3	9	5	3.5	3.5	
	b cm	13.6		9.3	7				
	V cc	656	91	1135	482	167	82	115	3092
	C cm	37		34.1					
1y	H cm	11	5.2	19.3	9.5	15	15	24	75
	a cm	12	6	16.5	19	7	5.5	4.8	
	b cm	16		10.5	11.15				
	V cc	1659	147	2626	1631	577	356	426	8779
	C cm	44.4		43.5					
5y	H cm	14	6	24.5	12.5	24	24	33	105
	a cm	13.5	6.5	18.8	21	8	6.2	5.4	
	b cm	17		12.5	12.5				
	V cc	2524	199	4450	2577	1208	725	756	15125
	C cm	48.2		50.2					
10y	H cm	14.2	8.4	29.8	15.2	31.3	31.3	43.2	130.2
	a cm	13.2	7.5	21.8	21.8	9	7.5	6.5	
	b cm	18.2		15.17	14.17				
	V cc	2674	371	7728	3681	1988	1381	1433	24058
	C cm	50		59					
15y	H cm	17.1	9.9	34.8	18.1	37.5	37.5	51.5	154.9
	a cm	13.8	9.8	25	25	10.5	9	7.5	
	b cm	18.9		19.53	18.1				
	V cc	3503	747	13346	6433	3248	2386	2275	39848
	C cm	52		70.1					
20y	H cm	19.1	9.9	36.8	19.1	39.5	39.5	53	164
	a cm	14.5	12.2	28	29	11.4	9.5	8	
	b cm	19.1		20.7	20.7				
	V cc	4155	1157	16730	9012	4032	2800	2664	50047
	C cm	53.2		77.3					



**Fig.11: Family of BOMAB phantoms**

radionuclide in the phantoms and measuring the emitted photons in a linear standing counting geometry to be used for routine monitoring. A set of 36, 33, and 30 point sources of <sup>133</sup>Ba (for <sup>131</sup>I), <sup>137</sup>Cs and <sup>60</sup>Co, respectively were used for calibration of Quick Scan WBM. The strength of these sources had been accurately determined within ±5%. The sources for each radio nuclide were distributed throughout the phantom of each age groups and response in terms of Calibration Factor (cps/Bq) were evaluated. The values of calibration factors for different age groups for the Quick Scan WBM are presented in the Table 3.

Importantly, to get the improved response from the system, a stand of 30 cm height is used on the subject platform above which the 1-, 5-, 10- years age group phantoms were kept whereas for age group of 15- and 20- phantoms were kept directly on subject platform and calibration factors were evaluated. The subjects with height ≤ 135 cm are to be monitored while standing on the stand provided inside the Quick Scan WBM, where as subjects with height ≥ 135 cm are to be monitored directly. The system response was also studied for the localized deposition of a radionuclide viz. <sup>131</sup>I in thyroid. For this purpose, a single source of <sup>133</sup>Ba was placed only in the neck part and the rest of the other containers of the phantoms were kept without source.

### Determination of Minimum Detectable Activity (MDA)

The MDA of QS-WBM for each age group for radio nuclides <sup>137</sup>Cs (661.7 keV), <sup>60</sup>Co (1173.2 & 1332.5 keV) and <sup>133</sup>Ba(356 keV) for a counting time of 1 and 3 minutes were calculated. The following expression was used for MDA calculations.

$$MDA (Bq) = \frac{2.707 + 4.65\sqrt{B}}{T * C.F.}$$

Where B is counts in the background region of interest with uncontaminated person, T is counting time in seconds and CF is calibration factor (cps/Bq) for radionuclide energy of interest for given age group.

### Conclusion

The Quick Scan WBM type systems are useful for rapid measurement of internal contamination if any, during normal as well as emergency situations and help in increasing throughput without compromising on the sensitivity. The system can monitor approximately 30 persons in an hour, which is optimized by taking into account, the requirements of emergency situations. Importantly, the use of the standing geometry allows the radiation workers to be turned and recounted from back if necessary for ensuring the type of contamination (external or internal). The ratio of counts of front to back part or top to bottom portion can be used to identify presence of external

**Table 3: Quick Scan WBM : Calibration Factors (cps/Bq) and Minimum Detectable Activity (MDA) for different radio nuclides for family of phantoms and BARC reference phantom**

Radio Nuclide	Energy (keV)	1- yr old age group			5- yr old age group			10- yr old age group			ALI <sup>+</sup> (Inhalation) Bq
		CF	MDA (Bq)		CF	MDA (Bq)		CF	MDA (Bq)		
		cps/Bq	1 min	3 min	cps/Bq	1 min	3 min	cps/Bq	1 min	3 min	
<sup>133</sup> Ba	356	4.60E-03	485	280	4.93E-03	452	261	4.36E-03	511	296	
<sup>137</sup> Cs	661.7	7.96E-03	218	122	8.99E-03	193	108	8.69E-03	200	112	3 × 10 <sup>6</sup>
<sup>60</sup> Co (I)	1173.2	6.60E-03	167	93	7.30E-03	151	84	6.93E-03	159	88	1.2 × 10 <sup>6</sup>
<sup>60</sup> Co (II)	1332.5	6.06E-03	162	93	6.20E-03	159	91	6.10E-03	162	93	1.2 × 10 <sup>6</sup>
<sup>131</sup> I	364	5.29E-03	422	244	5.67E-03	393	227	5.01E-03	445	257	1.8 × 10 <sup>6</sup>
<sup>131</sup> I Thy*	364	9.12E-03	245	141	9.40E-03	237	137	7.48E-03	298	173	1.8 × 10 <sup>6</sup>
Radio Nuclide	Energy (keV)	15- yr old age group			20- yr old age group			BARC Reference Phantom			ALI <sup>+</sup> (Inhalation) Bq
		CF	MDA (Bq)		CF	MDA (Bq)		CF	MDA (Bq)		
		cps/Bq	1 min	3 min	cps/Bq	1 min	3 min	cps/Bq	1 min	3 min	
<sup>133</sup> Ba	356	2.92E-03	763	441	2.67E-03	835	483	2.41E-03	925	535	
<sup>137</sup> Cs	661.7	6.09E-03	285	160	5.52E-03	315	176	4.72E-03	368	206	3 × 10 <sup>6</sup>
<sup>60</sup> Co (I)	1173.2	5.06E-03	218	121	4.80E-03	230	127	4.53E-03	243	135	1.2 × 10 <sup>6</sup>
<sup>60</sup> Co (II)	1332.5	4.53E-03	218	125	4.23E-03	233	133	4.15E-03	237	136	1.2 × 10 <sup>6</sup>
<sup>131</sup> I	364	3.36E-03	664	384	3.07E-03	726	420	2.77E-03	804	465	1.8 × 10 <sup>6</sup>
<sup>131</sup> I Thy*	364	7.40E-03	301	174	5.32E-03	419	242	5.22E-03	427	247	1.8 × 10 <sup>6</sup>

\* Source only in thyroid.

+ For reference worker

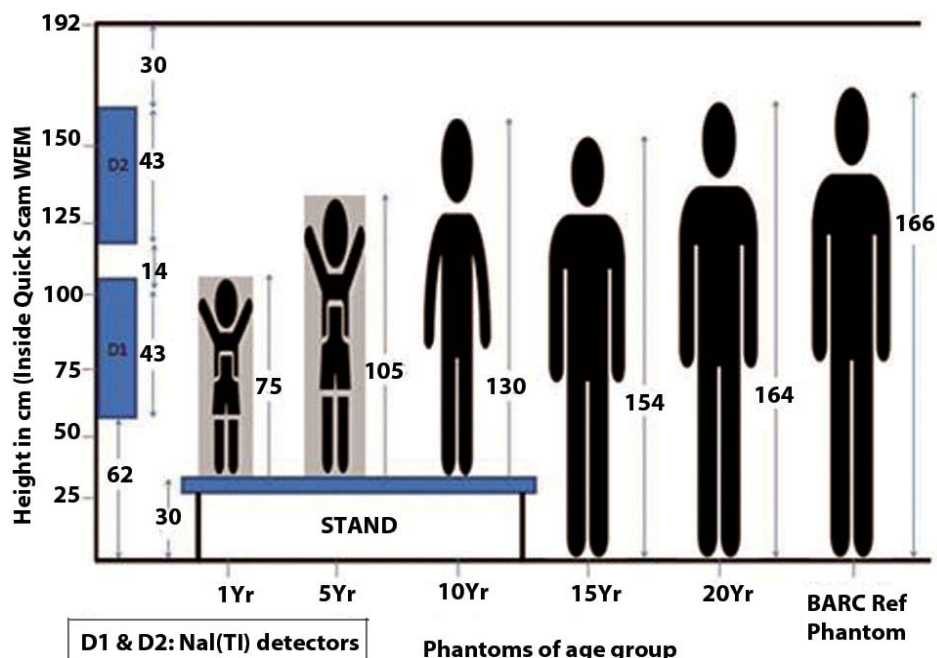


Fig.12: Schematic representation of different phantoms w.r.t detectors inside QS-WBM

contamination, if any. The calibration of the Quick Scan WBM using BARC reference and family of BOMAB phantoms representative of male Indian population provides for realistic and accurate evaluation of internal contamination. The observed MDAs for <sup>137</sup>Cs, <sup>60</sup>Co and <sup>131</sup>I are a small fraction of respective ALI values even for a 1 minute counting time.

**Acknowledgements**

Authors gratefully acknowledge the contribution of Shri D.Toppo, IDS, RSSD in this work at each stage of development and operation.

**References**

1. Direct Determination of the Body Content of Radionuclides. ICRU Report 69. J.ICRU 3(1)(2003)
2. Rapid Monitoring of large groups of internally contaminated people following a radiation accident. IAEA TECDOC-746. (Vienna:IAEA) (1994).
3. Mehta DJ, Singh I S, Sharma R C. A family of phantoms representative of male Indian population

for calibration of whole body counters. *RadiatProt Environ* (2003);26;327-32.

4. Singh I. S., Suri M.M.K.,Vidhani J.M., Garg S. P. and Sharma R. C. Development of an automated shielded chair whole body monitor. *Rad. Prot. Dosim.*102(2) 145-151 (2002).
5. Dang H.S, Jaiswal D.D., Parmeswaran M. and Krishnamony S. Physical Anatomical, Physiological & Metabolic data for Reference Indian Man. BARC/ 1994/E/043.
6. Sankhla R, Singh I S, Rao D D. BARC reference BOMAB phantom for calibration of whole body monitor, 32 national conference AMPCON-2011, Vellore;CMC;(2011).
7. L.A. Currie, "Limits for Qualitative Detection and Quantitative Determination".
8. Application to Radiochemistry. *Analytical Chemistry* 40(3):586-593; 1968.
9. IAEA Safety Series No.:114; "Direct methods for measuring radionuclides in the human body".

# Development of Ce doped $\text{Li}_6\text{Y}(\text{BO}_3)_3$ Crystal Based Portable Solid State Detectors for Thermal Neutrons

A.K. Singh, M. Tyagi, S.G. Singh, D.G. Desai, B. Tiwari,  
S. Sen, S.C. Gadkari and S.K. Gupta  
Technical Physics Division

## Abstract

Single crystals of Ce doped  $\text{Li}_6\text{Y}(\text{BO}_3)_3$  have potential applications to be used as a scintillator to detect thermal neutrons. These single crystals having an optimum Ce concentration been successfully grown using the Czochralski technique. The crystals have been characterized for optical and scintillation properties. A portable detectors set-up that works from a USB port of a laptop has been developed to detect thermal neutrons. The detection efficiencies in excess of 80% have been achieved even for thin slices of the crystal (1 mm thick) mounted on a photo-multiplier tube (PMT).

**Keywords:** Crystal growth, Scintillator, Neutron Detector.

## Introduction

Neutron detectors find several applications in research, defense, security and nuclear industries. The conventional neutron detectors are based on  $^3\text{He}$  and  $\text{BF}_3$  gas filled chambers. While  $\text{BF}_3$  is corrosive and toxic, the shortage of  $^3\text{He}$  has made it prohibitively expensive. Due to the dwindling supply of  $^3\text{He}$ , there is an urgent need to explore alternative detector materials. Solid state detectors based on inorganic scintillator single crystals are promising candidates and have the advantage of being portable and durable. These detectors would inherently have a better efficiency due to the higher atomic density compared to other conventional detectors based on gas chambers.

Single crystals of  $\text{Li}_6\text{Y}(\text{BO}_3)_3$  (LYBO) doped with cerium have been proven as a promising neutron scintillator. This material contains  $^6\text{Li}$  (natural abundance 7.4%,  $\sigma_{\text{abs}} = 940$  barns) and  $^{10}\text{B}$  (natural abundance 20%,  $\sigma_{\text{abs}} = 3835$  barns) that have large cross section for thermal neutrons and produce charged particles ( $^4_2\text{He}$  and  $^3_1\text{H}$ ) after interactions [1]. The alpha particles generated in  $^{10}\text{B}$  ( $n, \alpha$ )  $^7\text{Li}$  and  $^6\text{Li}$  ( $n, \alpha$ )  $^3\text{H}$  reactions excite the  $\text{Ce}^{3+}$  ions resulting in a fast and efficient emission at 420 nm. This emission matches well with the efficiency response of bi-alkali photomultiplier tubes (PMT) and therefore can be easily read out using standard electronics. A reasonable light output of about 1200ph/MeV enables efficient collection and a clean pulse height spectrum. A lower effective Z of the LYBO compared to other neutron scintillators also

helps impart insensitivity to gamma-rays that prevails in mixed field radiations [2].

## Experimental

The Ce doped single crystals of LYBO were grown using the Czochralski technique in an automatic diameter controlled crystal puller system (Model: Oxypuller, Cyberstar). The single phase starting charge was synthesized by solid state sintering of constituent oxides ( $\text{Li}_2\text{CO}_3$ ,  $\text{Y}_2\text{O}_3$ ,  $\text{H}_3\text{BO}_3$ ,  $\text{CeO}_2$ , 99.99% purity) taken in a stoichiometric ratio. The cerium concentration was taken 0.2 at% in the starting charge which could be lower in the grown crystal due to the segregation. A two step sintering at 700°C for 24 hours each was used with intermediate mixing. The formation of a single phase compound was confirmed by recording a powder XRD pattern employing a Rigaku RINT 2000 diffractometer [ $\text{Cu K}_\alpha$  radiation ( $\lambda = 1.545056$  Å)] with a step size of 0.02° in 2θ range of 10-80°. The synthesized charge in the form of pellets was loaded in a platinum crucible. An RF power supply was used to melt the material by induction heating. The power was adjusted to keep the temperature at about 50°C higher than the melting temperature to homogenize the melt which is recommended for the growth of this family of borates [3].

A seed crystal of LYBO was used to initiate the growth in argon ambient. The optimized growth parameters for the growth of LYBO crystal are listed in Table 1.

**Table 1: Crystal growth parameters**

Melting temperature	850°C
Pull rate	0.5 mm/h
Rotation rate	10-20 rpm
Ar gas pressure	1100 mbar (continuous flow)
Temperature gradient	~ 100°C/cm
Cooling rate	35-40°C/h

Transmission/absorption spectra were recorded with a Shimadzu 3600 UV-VIS NIR spectrometer in the range from 185 nm to 800 nm. Photoluminescence (PL) studies were performed over a wavelength range from 250 nm to 500 nm at room temperature employing a fluorescence spectrometer (Edinburg Model-FLP920). The emission was recorded in reflection geometry by positioning the sample at 45° with respect to the excitation beam. A steady state xenon lamp was used as an excitation source and a spectral bandwidth of 1 nm was selected for both excitation and emission arms. The recorded luminescence spectra were corrected for the spectral sensitivity function of the instrument. The scintillation decay was measured by recording the anode pulse from a PMT (Hamamatsu make, Model No. R2154) using a fast digital oscilloscope. The decay times resulted due to both neutrons and gamma exposures were measured. The Pulse height spectra (PHS) were recorded for thermal neutrons in a beamline of the Dhruva reactor. Various shields like lead brick and borated rubber was used to discriminate the spectra from neutron and gamma contributions. The spectra were also recorded at various fluxes of thermal neutrons from Am-Be and <sup>252</sup>Cf sources having known neutron fluxes. While <sup>252</sup>Cf sources generate fast neutrons via spontaneous fission, fast neutrons in Am-Be sources are generated by α particles (emitted from <sup>241</sup>Am) via the following reaction:



The fast neutrons are thermalized using graphite moderators.

## Results and Discussions

### Crystal growth

Fig.1 shows differential thermal analysis (DTA) plots of the synthesized charge. The melting and freezing behavior of the material indicates a large supercooling of more than 250°C which is common among the families of borates. Hence, the growth station was modified to achieve a higher temperature gradient of about 100°C/cm just above the melt.

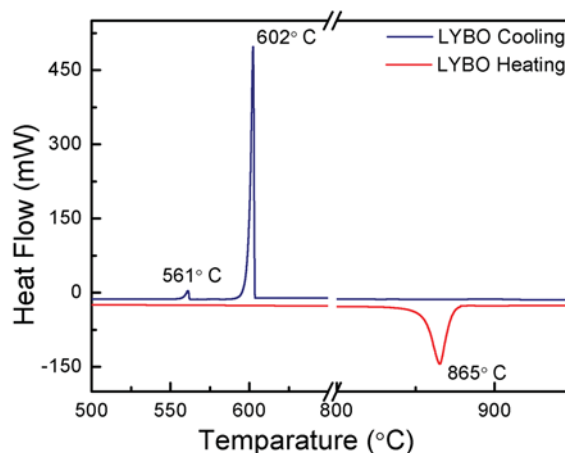


**Fig. 1: DTA plot of Ce doped LYBO**

The as-grown single crystal of LYBO is shown in Fig.2. The grown crystal was about 20 mm in diameter and 25 mm long. The crystal was free from any visible inclusion or impurity. Due to a high viscosity of the melt, the formation of bubbles is a common problem in these crystals which has been avoided by applying a higher temperature gradient and slow pull rates. Thus the crystals could be grown bubble-free as shown in the figure. A slow cooling rate was employed and the as-grown crystals were annealed at 500°C for 24 hours to reduce thermal stresses. This eventually helped to reduce cracking of crystals.



**Fig. 2: As-grown single crystal of Ce doped LYBO**

The powder XRD pattern of an as-grown crystal is shown in Fig.3. The phase of the material has been verified by the JCPDS data [4]. The lattice parameters have been calculated and found to match with the

reported data. The structure parameters for the LYBO crystal are listed in the Table 2

**Table 2: Crystal structure data of LYBO**

Structure	Monoclinic
Lattice parameters	a=7.15 Å, b=16.378 Å, c= 6.62 Å
Space group	P21/c

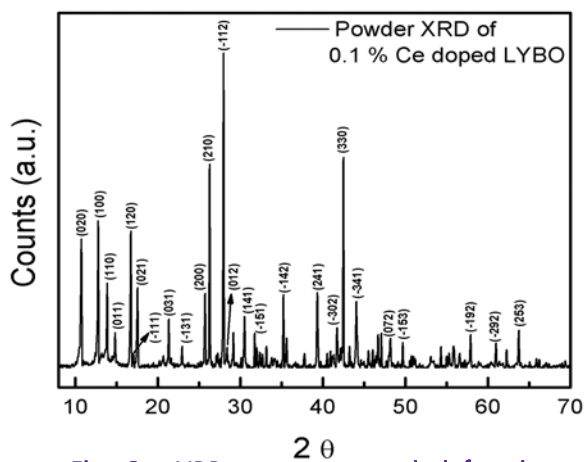


**Fig. 3: XRD pattern recorded for the powdered Ce doped LYBO crystal**

**Optical characterization**

The transmission spectrum for a polished sample (~2mm thickness) prepared from the as-grown crystal showed more than 80% transmission in the wavelength range from 185 nm to 1100 nm, as shown in Fig.4. The emission originating due to Ce<sup>3+</sup> centers at 420 nm is in the transmission region of this crystal as shown in the same figure. This indicates that the self absorption in these crystals will not be a serious problem. The α particles generated from (n, α) reaction cause ionization of Ce<sup>3+</sup> ions. A radiative de-excitation

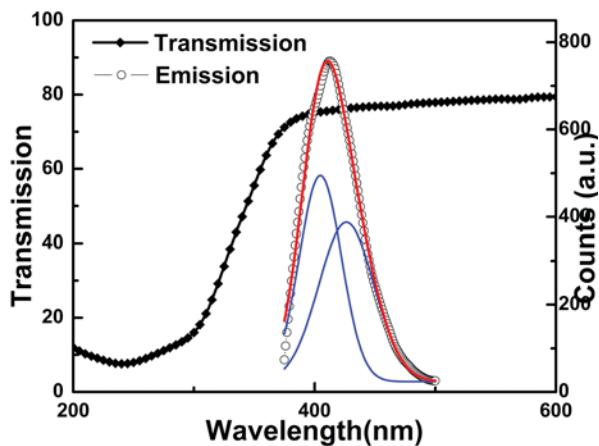


**Fig. 4: Transmission and emission spectra of LYBO:Ce crystal**

of electrons from 5d to 4f energy levels of Ce<sup>3+</sup> centers cause the emission band peaking at 420 nm. It mainly consists of two bands peaking at 390 nm and 410 nm due to splitting of <sup>4</sup>F<sub>5/2</sub> and <sup>4</sup>F<sub>7/2</sub> ground state [5].

This blue emission matches well with the response of a standard bi-alkali PMT and therefore a standard scintillation set up may be employed to record the pulse height spectra. The scintillation decay profiles of the crystal measured due to the excitation from gamma rays and neutrons are shown in Fig.5. A single exponential decay with a decay time of 27 ns for neutrons and 48 ns for gamma rays has been observed. Though the difference in the decay times by these two excitations is not significant, still it can

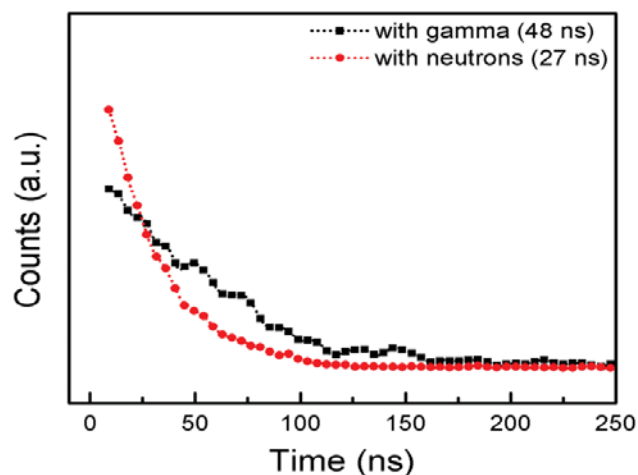


**Fig. 5: Scintillation decay profiles for the excitation of LYBO:Ce by gamma-rays and neutrons**

be useful to discriminate the gamma rays from neutrons by a suitable pulse shape discrimination technique.

**Setup for a USB powered neutron detector**

Scintillator discs of 10 mm diameter and about 1 mm thick were processed from the as-grown crystal. One face of the crystal was polished and optically coupled to a 1 inch diameter PMT (Hamamatsu make). The scintillator was wrapped with reflecting Teflon tapes and finally with aluminum foil. The reflecting tapes ensure efficient collection of light towards the PMT while Al foil minimizes the dark current of the PMT that may arise due to background light. The output from the PMT was given to a pulse processing chain consisting of a Pre-Amp, a shaping Amp and an 8k multi-channel analyzer (MCA). The power to all components including HV to the PMT was fed through a USB port of a laptop by employing suitable DC-DC converters. The data processing was done by the Amptek DppMCA software. The amplifier parameters

like shaping time, gain, LLD etc., were optimized to obtain a clean pulse height spectrum. A typical set-up used for recording the PHS is shown in Fig.6. The portability of the detector set-up makes it useful and an easy choice in various applications.

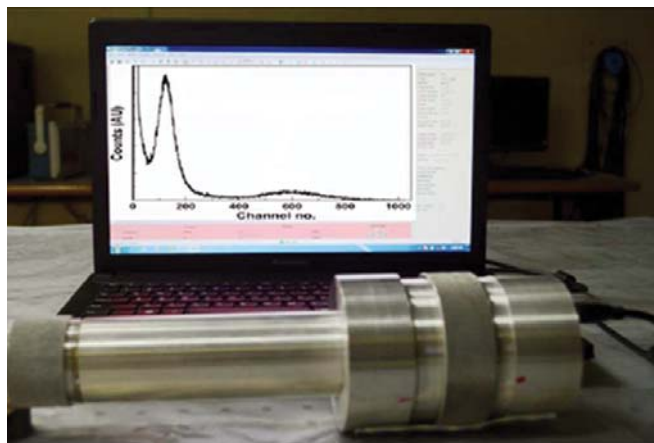
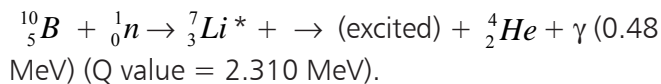


**Fig. 6: A photograph of a USB based neutron detector employing LYBO:Ce scintillator crystal**

**Performance characteristics of neutron detector**

The interaction of neutrons with LYBO crystals takes place via following reactions:

With <sup>10</sup>B



With <sup>6</sup>Li



The smaller size (~ 1 mm thickness) of the crystal was chosen to minimize the contribution from gamma background. However due to higher atomic density of lithium and boron atoms in these materials, the thickness is still sufficient to achieve good efficiency. The other important parameters of LYBO:Ce crystals are listed in Table 3. Pulse height spectra (PHS) recorded by this set-up for thermal neutrons from a Am-Be source is shown in Fig.7 [6].

The pulse height spectra comprised of two peaks near channel No. 190 and 950 corresponding to (n,α) reaction with <sup>10</sup>B and <sup>6</sup>Li, respectively. The integrated count for the two peaks have been calculated and found to be in agreement with the ratio of two fluxes within the standard deviation. With a neutron shield, the absence of these two peaks in the PHS, confirmed the origin as interactions of neutrons with the crystal.

**Table 3: Properties of LYBO:Ce crystal**

S.No	Properties	Numerical value
1	Neutron capture peak electron energy	2.22 ( <sup>6</sup> Li capture) 0.46 ( <sup>10</sup> B capture)
	equivalent (MeV)	
2	Scintillation decay time	27 ns (0.1 at.% Ce)
3	Density (gm/cm <sup>3</sup> )	2.8
4	Atomic density (10 <sup>22</sup> atoms/cm <sup>3</sup> )	3.28 ( <sup>6</sup> Li capture) 1.64 ( <sup>10</sup> B capture)
5.	Macroscopic capture cross section (cm <sup>-1</sup> )(at thermal)	30.9 ( <sup>6</sup> Li capture) 63.3 ( <sup>10</sup> B capture)
6.	Calculated neutron Detection efficiency (@ 0.025 eV) (1mm thickness)	~ 99.8 % Due to high atomic density of ~ 3 x 10 <sup>22</sup> atoms/cm <sup>3</sup> [1]

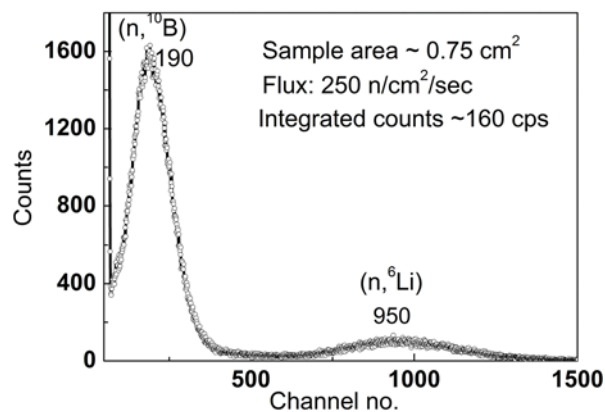


**Fig. 7: Measurement of pulse height spectra at from a thermal neutron source having known flux [6]**

It could be noted that although the alpha energies produced in the <sup>10</sup>B and <sup>6</sup>Li reaction are 1.47 MeV and 2.2 MeV respectively, the pulse height corresponding to <sup>6</sup>Li is about five times larger than that due to <sup>10</sup>B. This is because the generation of relatively light charged particles (<sup>3</sup>H & <sup>4</sup>He) in the case of <sup>6</sup>Li as compared to <sup>10</sup>B (<sup>7</sup>Li & <sup>4</sup>He) due to which a larger equivalent electron energy is deposited in the crystal for the nuclear reaction with <sup>6</sup>Li [1]. However the lower relative intensity of the peak due to lithium is due to a lower cross section as well as a lower abundance of <sup>6</sup>Li (about 7%) as compared to <sup>10</sup>B (about 20%) in the natural constituents used for the growth of the crystals. The PHS due to thermal neutrons in a beamline of the Dhruva reactor has also been recorded as shown in Fig.8.

The relatively poor resolution of the peak due to <sup>10</sup>B reaction can be attributed to heavy gamma background present in the reactor. Keeping a gamma shield makes the spectrum better. The peak due to <sup>6</sup>Li interaction can be enhanced several folds by using a

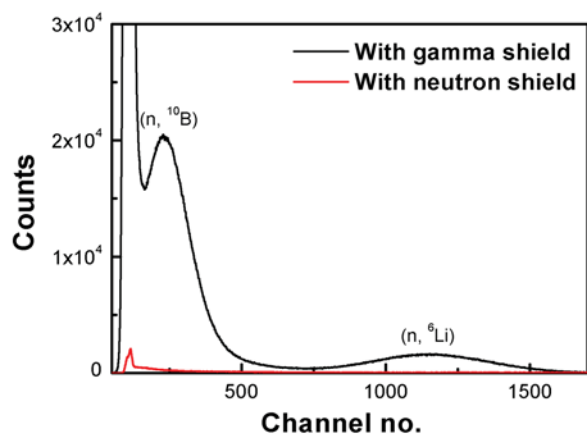


**Fig. 8: Pulse height spectra recorded for neutrons in a Dhruva reactor beamline**

material enriched in  ${}^6\text{Li}$  that would consequently lead to better pulse height discrimination from low energy gamma background.

### Conclusions

Defect-free single crystals of Ce doped LYBO were successfully grown. The grown crystals have been characterized for their phase and optical properties. Scintillation characteristics show their potential to detect thermal neutrons. After optimizing the scintillation parameter of the crystal, portable neutron detectors have been developed, which could be powered from a USB port of a laptop.

### References

1. B. Czirr, et al, *Nucl. Inst and Meth. A* 424 (2011) 15.
2. A. K. Singh, et al, *J Lumin.* 137 (2013) 208.
3. U. Fawad, et al, *Journal of Crystal growth*, 410 (2015)18-22.
4. JCPDS card No. 80-0843
5. A.M. Srivastava, et al, *Opt. Mater.* 32 (2010) 936.
6. A.K. Singh et al, *Nucl. Inst and Meth. A* (2015, in press).

## Special Session on the Eve of 100<sup>th</sup> Meeting of Conventional & Fire Safety Review Committee (CFSRC) of BARC Safety Council (BSC)

Pursuant to a gazette notification, a separate three tier internal safety framework with BARC Safety Council (BSC) at apex was established in May, 2000 for safety and regulatory coverage for the facilities and the projects under BARC. Conventional & Fire Safety Review Committee (CFSRC), in second tier of the review system, assisted by several Unit Level Safety Committees (ULSCs) and special committees, carries out regulatory review of all the conventional and non-radiological facilities, laboratories and general areas falling under the purview of BARC within the country.

In view of commemorating the 100<sup>th</sup> Meeting of CFSRC, a special session was held on August 26, 2015 at 'C' Block Auditorium, Mod Labs with an endeavor for further upliftment of safety status in the facilities. Former Chairmen and Member-Secretaries of the committee and other prominent officials who were earlier associated with CFSRC and contributed significantly towards efficient functioning of the committee were invited to share their experience with the existing members of all the ten ULSCs and four special committees under the aegis of CFSRC. The programme was graced by Dr. S. Banerjee, Former Chairman, AEC who had also been Chairman, CFSRC and other dignitaries like Shri G. P. Srivastava, Former Chairman, BSC; Shri G. Gouthaman, Former Chairman, BSC; Shri S. G. Markandeya, Former Chairman, CFSRC; Shri R. P. Raju, Controller, BARC; Shri Y.K.Taly, Chairman, BSC and Shri Jose Joseph, Head, BSC Secretariat also graced the occasion.

In introductory note, Shri S.K.Garai, Member-Secretary, CFSRC presented the historical perspective of the formation of three tier internal safety framework under BSC and informed that over the time, BSC, under the guidance of Director, BARC has established a full-fledged safety review mechanism for all the operating facilities and the upcoming projects.

Shri Jose Joseph, in his welcome address, expressed his pleasure to welcome all the luminaries to the inaugural session and articulated his gratefulness to Director, BARC

for readily concurring with the proposal for holding the meeting in an elaborate and reflective manner. He remarked that CFSRC along with several ULSCs under its purview has acted as a catalyst in maintaining high level of conventional safety in BARC. He reiterated the importance of the meeting in consolidating feedback from concerned officers to strengthen activities of CFSRC further.

Shri Y.K.Taly reiterated that a regulatory body promotes an effective safety management system, monitors the performance and enforces regulations to strengthen the safety management system in the organization and safeguard any deterioration in safety performance. The internal safety framework under BSC aims to achieve incident-free operation of the facilities for protecting working personnel, members of public and environment against any danger including the probable harmful effects of radiation. It has established a comprehensive regulatory review process for all the BARC facilities and to a great extent ensures that safety does not get compromised at any stage of the operation.

Shri S.G.Markandeya shared his experience and views he gathered during his tenure of chairmanship in 20 meetings of CFSRC. He attributed in CFSRC's accomplishment of ensuring very high level of safety in the BARC facilities to thorough review of design, safety analysis, excellent documentation and periodic inspections by Regulatory Inspection Teams, but recommended continuous update in the light of evolving state-of-the-art knowledge. He emphasized that imbibing strong safety culture among all the staff members and further strengthening the regulatory body with executive powers for imposing graded



**Dignitaries contemplating over the issues**



Dignitaries addressing the special session

punitive actions on safety violators can be the key to achieve incident free safety environment.

Shri R.J.Patel, Chairman, CFSRC explained that this special session is convened to provide a platform to all existing members to interact with the former members and making use of their accumulated experience to meet the prevailing standard in the operating and upcoming facilities and thereby uplifting the safety status of the centre as a whole. He reiterated that due to the persistent efforts of CFSRC, safety has got widespread recognition in various facilities and safety performance has been continuously improving over the years since the inception of BSC. He updated about thrust given for resolution of many issues long pending for safety clearance.

Shri R.P.Raju applauded the effort put forward by CFSRC in ensuring overall safety standard in BARC facilities. He further expressed his satisfaction in the fire audit scheme devised by CFSRC and overall fire safety compliance in BARC buildings.

Shri G.Gouthaman congratulated CFSRC for achievements of various milestones over the years and stressed to evaluate quantitative assessment while conducting Regulatory Inspections of the facilities. He further emphasized on undertaking the structural audit of the old buildings in BARC.

Shri G.P.Srivastava shared his pleasure in efficient functioning of BSC, updating various statutory rules and requirements. He stressed the need for interlinking safety with security as

these are complementary to each other and expressed his happiness for initiating the right steps taken by BSC in this direction. He further emphasized on proper integration of safety review procedures in the facilities with respect to radioactivity as well as from the point of conventional and fire safety aspects.

Dr. S. Banerjee was introspective in his address and expressed his satisfaction in overall performance of CFSRC in resolving various issues. He reiterated that safety, in general, is an integral part of everyday life but to ensure safety in facilities, plants and industries, focused attention should be ensured. He further stressed that the facilities should be upbeat in preventing even the freak incidents and the safety committees under BSC, with their vast knowledge and experience in safety regulation should also play a proactive role in national arena.

After the inaugural session, Chairpersons and Member-Secretaries of various ULSCs presented the elaborated feedback and the several achievements of the committees which includes compliance of recommendations of safety committees, changes and modifications carried out in the systems, violation of Technical Specifications, Significant Event Reporting, Industrial and Fire Safety, documentation, performance of engineered safety features, compliance of previous RIT recommendations, Waste Management, safety training, ensurance of health and hygiene for canteen staff and emergency preparedness of the facilities, apart from issuance of recommendations for safety clearance of various facilities. CFSRC acknowledged and appreciated the relentless efforts and contributions of the ULSCs and other special committees in raising overall safety standard and further reiterated to be more proactive in complying with the recommendations in a time-bound manner. The session was concluded with profound appreciation from the participants and dignitaries.



Dignitaries and participants

## Technology Transfer to Industries

During the period between May 2015 and July 2015, BARC has transferred Eleven technologies to various industries. Technology Transfer & Collaboration Division (TT&CD) co-ordinated these technology transfers. The details are given below:

**A. Solar Energy Driven Portable Domestic Brackish Water Reverse Osmosis (BWRO)" & "Stand-Alone Solar Photovoltaic (PV) Driven Battery-Less Ultra-Filtration (UF) Units For Water Purification" technologies were transferred to M/s Reveille Allied Engineers Pvt. Ltd., Visakhapatnam (AP) on May 25<sup>th</sup>, 2015.**

• **"Solar Energy Driven Portable Domestic Brackish Water Reverse Osmosis (BWRO)" Technology:**

The technology has been developed by Desalination Division, BARC. This technology is based on solar photovoltaic (PV) system hence it is battery-less, off-grid/stand-alone. It has capacity of 10 liters/hr (lph) which can desalinate contaminated water of salinity 1000 - 3000 ppm (mg/lit) to provide drinking water of 50 - 300 ppm. The product water will be devoid of toxic elements, pathogens & turbidity too. It is best suited for remote/rural areas where electricity is not available or the voltage is not stable. It can be used in urban areas also. As it is portable, it will be of great help for the people working in desert areas especially in the case of defense personnel.



Photograph after signing the agreement with M/s Reveille Allied Engineers Pvt. Ltd., Visakhapatnam (A. P.), seen from left to right, Shri V. K. Upadhyay, TT&CD, Shri S.N. Dutta, TT&CD, Dr. (Smt.) S. B. Roy, Associate Director, Chemical Engg. Group, Shri Sitaram Nadimpalli, Director, M/s Reveille Allied Engineers Pvt. Ltd., Visakhapatnam, Shri G. Ganesh, Head, TT&CD, Shri D. Goswami, Head, DD, Shri S. S. Ram, DD.

• **"Stand-Alone Solar Photovoltaic (PV) Driven Battery-Less Ultra-Filtration (UF) Units For Water Purification" Technology:**

The technology has been developed by Desalination Division, BARC. These units are solar photovoltaic (PV) driven, battery-less, off-grid, stand-alone Ultrafiltration (UF) systems for water purification. On sunny days, they can be operated for 9 – 10 hours/day. They are capable of removing un-dissolved species such as, dust, turbidity, microorganisms etc. from drinking water. These units are best suited for remote/rural areas where electricity is not available or the voltage is not stable. They can be used in urban areas also. As they are portable, they will be of great help for people working in desert areas, as in the case of defense personnel

**B. "Distress Alarm Device – NIRBHAYA; & "Distress Alarm Device – NIRBHAYA-GSM" Technologies were transferred to M/s. Nucleonix Systems Pvt. Ltd., Hyderabad (A.P) on June 6<sup>th</sup>, 2015.**

Electronics Division has developed compact low cost devices used in case of any distress like fear of attack or medical emergency to send information to near and dear ones including police. The devices have been developed with two different technologies.

• **"Distress Alarm Device – NIRBHAYA" Technology:**

As the name indicates The NIRBHAYA device is for safety and security of individuals. This Compact (2.2" x 1.4" x 0.7") device weighs only 45gms, can be carried in pocket or purse and is paired with user's cell phone via Bluetooth link. Since the device has on board GPS chip, it can be used in conjunction with a basic mobile handset. The device is very easy to use having only one switch. In case of need, when the switch is pressed, the device sends SMS alerts through user's mobile to pre-selected five cell phone numbers. The SMS alert contains user information and GPS location of the device. The device is rugged and cannot be destroyed easily.

• **"Distress Alarm Device – NIRBHAYA-GSM" Technology:**

BARC has developed a GSM based Distress Alarm Device called "NIRBHAYA-GSM". The user can send an SMS to his/her near and dear ones, when in distress

using this instrument. The instrument can be programmed to send SMS to up-to five user-defined numbers. The Distress SMS includes the users name, age, sex, blood group, and specific medical condition if any, in addition to the current GPS location of the user. User can also include conditions like "allergies to a particular medicine" in the medical condition while programming the instrument. The instrument can also respond to the queries from any one of the predefined numbers regarding the current user location. This is very useful in case of children or young persons who might be kidnapped or under distress but cannot use the instrument. It can be used for tracing goods & vehicles. This would also be beneficial for old persons suffering from memory loss conditions like Alzheimer or Parkinson.



Photograph after signing the agreement with M/s. Nucleonix Systems Pvt. Ltd., Hyderabad, seen from Right to left, Shri Gopal Joshi, Head, ACSS, Shri Rajesh Jain and Shri S K Lalwani, all from ED, Shri G Ganesh, Head, TT&CD, Shri C K Pithawa, Dir, E&IG, Shri Vineet Sinha, ED, Shri J. N. Reddy, MD, M/s Nucleonix, Shri S K Bharade, ED, Shri Debashis Das, Head, ED, Smt. Smita Mule, TT&CD, Shri. Shailesh Khole and Shikha Srivastava, ED

**C. "D/H Mass Spectrometer" Technology was transferred to M/s AUTOSYS, Mumbai, on June 23<sup>rd</sup> 2015.**

This technology of was developed by Technical Physics Division, BARC. The D/H Mass Spectrometer is a versatile analytical instrument. It is used for routine measurement of Deuterium/ Hydrogen ratio in water and hydrogen sample. It consists of sample inlet system, electron impact ion source, analyzer and faraday cup collectors. The sample inlet system consists of online reduction system for water samples & an inlet system for gas samples. The electron impact ion source is designed to have high sensitivity and low H<sub>3</sub> formation. The mass analyzer has a radius of 6 cm with deflection angle of 60°. Two independent collector assemblies have been incorporated to collect H<sub>2</sub> and HD ions. It operates around a base pressure

of 10<sup>-8</sup> torr. The vacuum system of it consists of rotary pump, turbo molecular pump and ion pump to achieve the vacuum of 10<sup>-8</sup> torr. PC based interface is provided for instrument control & sample analysis.



Photograph after signing the agreement with M/s AUTOSYS, Mumbai, seen from left to right, Shri V. K. Upadhyay, TT&CD, Shri S. N. Dutta, TT&CD, Shri S. K. Sahu, TPD, Shri A. M. Kasbekar, TPD, Shri Rabi Dutta, TPD, Shri V. Natraju, TPD, Shri R. B. Ingole, TPD, Shri P. S. Sarode, Proprietor, M/s AUTOSYS, Shri G. Ganesh, Head, TT&CD, Dr. S. L. Chaplot, Director, Physics Group, Dr. S. K. Gupta, Head, TPD, Shri M. M. Gulhane, TPD, Shri R. G. Ochani, TPD.

**D. "Preparation of Composite Polyamide Reverse Osmosis Membrane for Brackish Water (BWRO) Desalination" Technology was transferred to M/s Aqua Dynamic Solution, Malkapur (M.S), on June 26<sup>th</sup> 2015 and M/s Osmotech Membranes Pvt. Ltd., Rajkot (Gujarat), on July 03<sup>rd</sup>, 2015.**

This technology of was developed by Membrane Development Section, Chemical Engineering Group, BARC. Reverse osmosis (RO) is an efficient desalination technology for providing safe drinking water from brackish and sea water. Brackish water desalination is very common nowadays as most of the surface water available is brackish water. With proper collection and utilization, the reject stream can also be beneficially utilized. Membrane is the key component of the desalination process. BARC is engaged in the research and development of membrane preparation, assembling in different configurations and applications in various fields. Earlier BARC has developed and transferred the technologies for UF membranes. Technology for rolling of these membranes in spiral module has also been transferred. Present technology is developed for thin film based composite polyamide membranes and prototype 2512 spiral module. These membranes are capable of removing 90% salinity from brackish water (~feed concentration upto 3000 ppm). Using the developed technology, commercial size flat sheet membranes can also be made.



Photograph after signing the agreement with M/s Aqua Dynamic, Malkapur, seen from left to right, Shri V. K. Upadhyay, TT&CD, Dr. A. K. Ghosh, MDS, Dr. R. C. Bindal, Head, Membrane Development Section, ChEG, Shri Sanmati Jain, Pariner, M/s Aqua Dynamic, Shri G. Ganesh, Head, TT&CD, Shri Rahul Rane, Partner, M/s Aqua Dynamic, Shri S. N. Dutta, TT&CD.



Photograph after signing the agreement with M/s Osmotech Membranes Pvt. Ltd., Rajkot, seen from left to right, Dr. A. K. Ghosh, MDS, Dr. R. C. Bindal, Head, Membrane Development Section, ChEG, Shri Shreyas J. Vagadia, Director, M/s Osmotech Membranes Pvt. Ltd., Shri G. Ganesh, Head, TT&CD, Shri V. K. Upadhyay, TT&CD and Shri S. N. Dutta, TT&CD.

**E. "Optical Spectrometer" Technology was transferred to M/s Prisms India Pvt. Ltd., Pondicherry, on July 8<sup>th</sup> 2015 and M/s New Age Instruments & Materials Pvt. Ltd., Gurgaon, Haryana on July 28<sup>rd</sup>, 2015**

The optical spectrometers developed by Precision Engineering Division are for 600-1100 nm & 700-900 nm wavelength range. These spectrometers are based on Diffraction Grating and Linear Image Sensor. As there is no mechanical scanning through rotation of grating to capture the spectrum, it makes such spectrometers fast and wear free. The spectrum can be seen in graphical format, recorded & analyzed

on computer with User Interface Software. Optical spectrometers find applications in various fields of science & technology.



Photograph after signing the agreement with M/s Prisms India Pvt. Ltd., Pondicherry, seen from Right to left, Shri Prabhat Ranjan, Shri Shivam Mishra & Smt. Shrinkhla all from PED, Shri. G. Ganesh, Head, TT&CD, Shri. S. Sarkar, AD ChTG and Head, PED, Shri. V. Jayaram, MD, Prisms India Pvt Ltd, Dr. Balasubramanian, Head, Precision Machining Section, PED, Smt Smita Mule, TT&CD



Photograph after signing the agreement with M/s New Age Instruments & Materials Pvt. Ltd., Gurgaon, seen from Right to left, Shri Prabhat Ranjan and Shri Shivam Mishra from PED, Shri. Sameer Sharda, Group Manager, Shri Tapan Sharda, Director, New Age Instruments & Materials Pvt, Ltd, Gurgaon, Shri. G. Ganesh, Head, TT&CD, Shri. S. Sarkar, AD ChTG and Head, PED, Smt Smita Mule, TT&CD and Smt. Shrinkhla, PED.

**F. "ChemoMechanical Magneto Rheological Finishing Machine (CMMRF)" Technology was transferred to M/s WENDT (India) Limited, Hosur on July 14<sup>th</sup>, 2015.**

Precision Engineering Division has developed a novel nanofinishing system which is named as 'ChemoMechanical Magneto Rheological Finishing (CMMRF) Machine' for achieving surface finish in order of few angstroms to few nanometers in various engineering materials. It is a hybrid finishing technology of chemical mechanical polishing (CMP)

and magneto-rheological finishing (MRF) technologies. CMMRF has capability to generate atomistic surface with flexibility of the process itself. CMMRF has polishing capacity of typically 0.5nm surface finish (Ra) in 50mm surface area of silicon material. It finds applications in General optics, LASER Optics, Soft X-ray Optics, Hard X-ray Optics, LINAC RF Cavity etc.



Photograph after signing the agreement with M/s WENDT (India) Limited, Hosur, seen from Right to Left, Shri Shivam Mishra, PED, Dr Anway Maiti, AGM(R&D), WENDT (India) Ltd, Hosur, Shri. Prabhat Ranjan, PED, Shri. G. Ganesh, Head, TT&CD, Shri. Rajesh Khanna, CE, WENDT (India), Shri. M. S. Venkatesh – Unit Head, WENDT, Dr Balasubramanian, Head, Precision Machining Section, PED, Smt Smita Mule, TT&CD and Ms Shrinkhla Ghildiyal, PED.

**G. “Mass Multiplication Medium for Biofungicide Trichoderma Spp.” Technology was transferred to M/s. Borlong Biotechnologies Pvt. Ltd., Lucknow on July 30<sup>th</sup>, 2015.**

Excess utilization of chemical insecticides has reduced fertility of soil, caused pollution of water and given rise to resistant pest varieties. To counter ill effects of



Photograph after signing the agreement with M/s. Borlong Biotechnologies Pvt. Ltd., Lucknow, seen from left to right, Dr S T Mehetre, Dr P. Mukherjee, NA&BTD, Shri G Ganesh, TT&CD, Dr S P Kale, AD (A), BSG and Dr Y Singh, Dir, Borlong Biotech Pvt Ltd., Lucknow.

chemicals on environment, bio-pesticides are being used on large scale. One such bio-pesticide is fungus- *Trichoderma*. Currently, sorghum or bajra grains are used for commercial production of *Trichoderma* spp. However their high cost and unavailability is limiting their use. Nuclear Agriculture and Biotechnology Division, BARC has developed an alternate and cheaper medium for mass multiplication of fungus *Trichoderma* using agriculture waste.

**H. Nisargruna Biogas Technology based on biodegradable waste** has been developed by NA&BTD. The plant processes biodegradable waste into biogas and weed free manure. It was transferred to the following six parties :-

- M/s. PriMove Engineering Pvt. Ltd., Pune, on 05.06.2015
- M/s. NextEra Energy Resources, LLP, Hyderabad on 10.07.2015
- M/s. Amalgan Ecotech LLP, Thane on 10.07.2015

**I. BARC through its Centre for Incubation of Technology has signed the MoU with M/s Innovative Drug Research Solutions, Labs, Bangalore for incubation of “Development of Radioprotector Drug” technology on July 10<sup>th</sup>, 2015.**

RB&HSD has developed a novel radioprotector compound with promising laboratory results. M/s IDRS Labs shall collaborate with BARC in the development of a marketable drug using various formulations of the compound.

The company is a winner of “Indian Leadership Award for Industrial Development” for the year 2014 - awarded by AIAF, Delhi, India and works.



Photograph after signing the agreement with M/s Innovative Drug Research Solutions, Labs, Bangalore, seen from right to left, Shri Yogesh Bhandari, Director IDRS Labs, Shri Pradeep Karatgi, Director IDRS Labs, Shri Shivkumar Madki, Managing Director, IDRS Labs, Shri G Ganesh, Head, TT&CD, Dr S. Chattopadhaya, AD (B), BSG, Dr Santosh Kumar, RB&HSD, Dr Deepak Sharma, RD&HSD, Dr V Gota, ACTREC and Dr N Khalap, TT&CD.

## BARC Scientists Honoured

**Name of the Scientists** : G. Pandey, R. Chichale, A.U. Renjith, S. Dixit, S. Mukhopadhyay, K.T. Shenoy and S.K. Ghosh  
**Affiliation** : Chemical Engineering Group  
**Name of Award/Honour** : 2<sup>nd</sup> Prize in Poster Presentation  
**Title of the Paper** : Extraction of Zirconium from Simulated Acidic Nitrate Waste using Liquid Membrane in Hollow Fiber Contactor  
**Presented at** : Trombay Symposium on Desalination & Water Reuse (TSDWR-2015), Mumbai, Jan. 22-23, 2015



**Dr. V.V. Parkar**

**Vivek Vijay Parkar**, Nuclear Physics Division has been awarded the INSA Medal for Young Scientist 2015 for his contributions in nuclear reaction measurements using weakly bound  ${}^6\text{Li}$  and  ${}^9\text{Be}$  projectile on a range of targets.



**Edited & Published by:**  
**Scientific Information Resource Division**  
**Bhabha Atomic Research Centre, Trombay, Mumbai - 400 085, India**  
**BARC Newsletter is also available at URL:<http://www.barc.gov.in>**